Activity of Sulfonium Bisphosphonates on Tumor Cell Lines

Yonghui Zhang,[†] Michael P. Hudock,[§] Kilannin Krysiak,[†] Rong Cao,[§] Kyle Bergan,[†] Fenglin Yin,[§] Annette Leon,[§] and Eric Oldfield*[,†,§]

Department of Chemistry, University of Illinois at Urbana-Champaign, 600 South Mathews Avenue, Urbana, Illinois 61801, and Center for Biophysics and Computational Biology, University of Illinois at Urbana-Champaign, 607 South Mathews Avenue, Urbana, Illinois 61801

Received August 9, 2007

We investigated three series of sulfonium bisphosphonates for their activity in inhibiting the growth of three human tumor cell lines. The first series consisted of 6 cyclic sulfonium bisphosphonates, the most active species having an (average) IC_{50} of 89 μM. The second consisted of 10 phenylalkyl and phenylalkoxy bisphosphonates, the most active species having an IC_{50} of 18 μM. The third series consisted of 17 n-alkyl sulfonium bisphosphonates, the most active species having an IC_{50} of ~240 nM. Three QSAR models showed that the experimental cell growth inhibition results could be well predicted. We also determined the structures of one sulfonium bisphosphonate bound to farnesyl diphosphate synthase, finding that it binds exclusively to the dimethylallyl diphosphate binding site. These results are of interest since they show that sulfonium bisphosphonates can have potent activity against a variety of tumor cell lines, the most active species having IC_{50} values much lower than conventional nitrogen-containing bisphosphonates.

Introduction

Bisphosphonates are an important class of drug molecules, used to treat a variety of bone resorption diseases, such as osteoporosis, Paget's disease, and hypercalcemia due to malignancy. In addition, some bisphosphonates have direct activity against cancer cells, both *in vitro*[1−5] and *in vivo*,[4,6−8] while others have antiparasitic[9] and antibacterial activity.[10] Bisphosphonates can also activate $\gamma\delta$ T cells (containing the Vγ2Vδ2 T cell receptor) of the immune system, and such activated T cells have both antitumor[11−13] as well as antibacterial activity.[14] There is, therefore, interest in the further development of bisphosphonates, for a variety of indications. The early development of bisphosphonates has been somewhat unusual in that it did not follow the current paradigm of target identification → drug discovery. Indeed, as noted by Reszka and Rodan,[15] bisphosphonates were used to treat bone resorption diseases for over 20 years without understanding their mechanism of action. Their discovery came about in early work,[16] in which it was shown that the simple molecule (or ion) diphosphate (**1**) had an effect on hydroxyapatite formation and stability, but the hydrolytic instability of diphosphate prevents its use as a bone antiresorption drug.

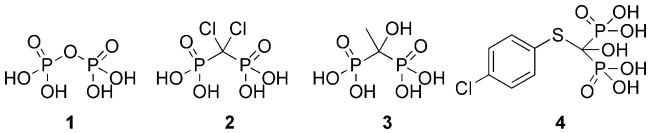

1 **2** **3** **4**

Consequently, nonhydrolyzable analogues of diphosphate, such as the methylene bisphosphonates clodronate (**2**), etidronate (**3**), and tiludronate (**4**), were developed, and these represent the so-called "first generation" bisphosphonates, used primarily to treat osteoporosis, although their molecular targets (which are different to those of modern bisphosphonates) were not known at the time of their introduction. Much later, these compounds were shown to be converted into cytotoxic analogues of ATP,[17] such as **5**: which act (in osteoclasts) by inhibiting

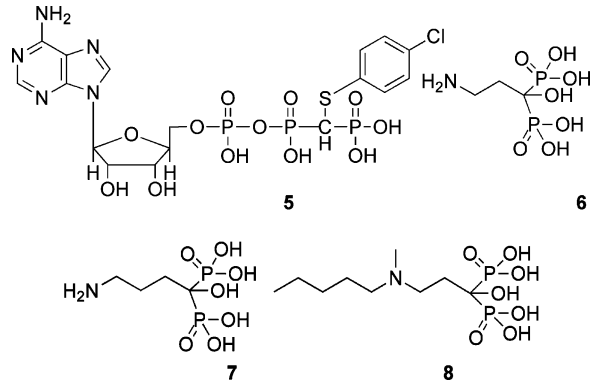

5 **6**

7 **8**

the mitochondrial ADP/ATP translocase,[18] leading to osteoclastic inactivity and, potentially, apoptosis. The doses of each of these drugs required for efficacy are, however, quite high, which led to the development of "second generation" bisphosphonates, such as pamidronate (**6**), alendronate (**7**), and ibandronate (**8**). These species all contain nitrogen and are generally referred to as NBPs[a] or nitrogen-containing bisphosphonates. Their mechanism of action differs from that of the non-nitrogen containing bisphosphonates (such as **2**, **3**) and involves inhibition of the enzyme farnesyl diphosphate synthase[15,19−22] (FPPS, EC 2.5.1.10). This enzyme is involved in the formation of farnesyl diphosphate (FPP), which is used by cells in protein prenylation, heme a, dolichol, and ubiquinone biosynthesis. In more recent work, aromatic-containing NBPs such as risedronate (**9**), zoledronate (**10**), and minodronate (**11**) have been developed, although minodronate is not currently marketed.

These aromatic NBPs are the most active bisphosphonates in bone resorption, have IC_{50} values of ~2 nM versus the human FPPS target, and are generally referred to as "third generation"

* Corresponding author. Phone: 217-333-3374. Fax: 217-244-0997. E-mail: eo@chad.scs.uiuc.edu.
[†] Department of Chemistry.
[§] Center for Biophysics and Computational Biology.

[a] Abbreviations: FPP, farnesyl diphosphate; FPPS, farnesyl diphosphate synthase; IPP, isopentenyl diphosphate; NBP, nitrogen-containing bisphosphonate; NNBP, non-nitrogen-containing bisphosphonate; QSAR, quantitative structure−activity relationship.

10.1021/jm700991k CCC: $37.00
Published on Web 10/27/2007

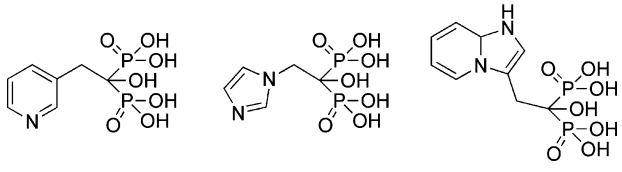

9 **10** **11**

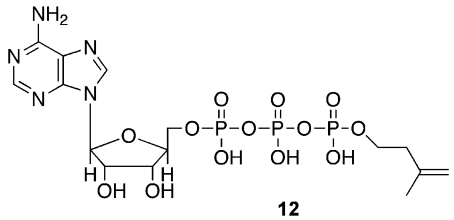

12

bisphosphonates. As with the other NBPs, their primary mechanism of action is thought to be in inhibiting FPPS, resulting in decreased protein (Rho, Ras, Rap 1A) prenylation,[23,24] and in most cases, enzyme inhibition also leads to formation of a strongly apoptotic species, the isopentenyl ester of ATP (**12,** ApppI),[18] produced from the isopentenyl diphosphate which accumulates.

From a structure/function perspective, we proposed early on that NBPs might be efficacious simply because, in their protonated-nitrogen forms, they would closely resemble the likely cationic transition state/reactive intermediate[20] formed during the FPPS catalytic cycle. For example, the protonated form of ibandronate (**8**) might mimic the carbocation formed from geranyl diphosphate (**13**):

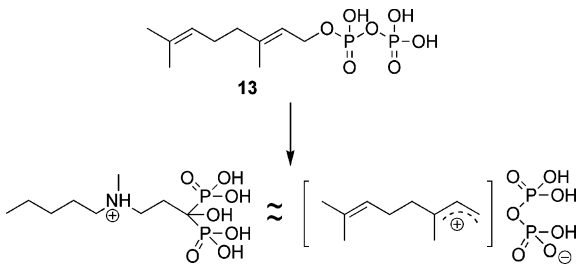

13

a view now supported by a wide variety of X-ray crystallographic studies,[25−27] as well as by NMR spectroscopy,[28] the latter technique providing direct evidence for the presence of charged side chains for NBPs bound to FPPS. This then leads to the idea that it might be worth investigating other cationic species, such as sulfonium, phosphonium, pyridinium, and guanidinium bisphosphonates, since some might have improved activity or other beneficial properties (e.g., improved lipophilicity). Here, we report the results of an initial investigation of sulfonium bisphosphonates, chosen for investigation at least in part because the S−Me sulfonium fragment occurs in common metabolites such as *S*-adenosylmethionine,[29] as well as in drugs such as suplatast.[30,31] We synthesized and tested a structurally diverse range of 33 sulfonium bisphosphonates, determined their activities in three tumor cell lines, and used QSAR methods to analyze the results obtained. We also determined the X-ray crystallographic structure of one sulfonium bisphosphonate, bound to FPPS, and used computational docking to see how others might bind.

Results and Discussion

General Strategies. There is now strong evidence that all of the commercially available nitrogen-containing bisphosphonates act, primarily, by inhibiting the enzyme farnesyl diphosphate synthase, binding to the allylic (dimethylallyl diphosphate or geranyl diphosphate) substrate binding site.[25−29] The bisphosphonate moieties undergo strong electrostatic interactions with three Mg^{2+} (which bind to a highly conserved DDXXD motif in the active site), while the cationic center is stabilized by the more diffuse electrostatic potential provided by a network of electronegative groups, with additional stabilization in some cases being provided via hydrophobic/van der Waals attractive interactions with hydrophobic amino acid side chains in the distal part of the allylic binding site. The most potent NBPs in tumor cell growth inhibition have been shown to be zoledronate (**10**) and minodronate (**11**), which we find have mean IC_{50} values of 15 ($\pm$7.3, $N = 63$) and 7.9 ($\pm$5.1, $N = 8$) μM, respectively, against three human tumor cell lines (NCI-H460 lung, MCF-7 breast, and SF-268 CNS), in good accord with the results obtained by other workers on a broad array of cell lines.

The question then arises as to how it might be possible to enhance activity in cell-based assays. There would seem to be at least four possibilities. First, it might be possible to "mask" the highly hydrophilic phosphonate groups by esterification,[32] and indeed in some cases this is possible, although in general this approach is synthetically challenging and also requires that the protecting group be cleaved in the cell. A second strategy is to enhance the lipophilicity of the cation by varying the nature of the cationic center, e.g., $N^+H_2 \rightarrow N^+HMe \rightarrow S^+Me \rightarrow P^+Me_2$. A third approach might be to vary the actual locus of the cationic center. As can be seen in the Introduction, the earlier generation NBPs (pamidronate, alendronate) have primary ammonium charge centers at γ and δ positions in the side chain, but these compounds have relatively poor activity (IC_{50} values of $\sim$200−300 μM) in tumor cell growth inhibition assays. The more potent species, zoledronate and minodronate, have more delocalized charges, and in the case of zoledronate, one of the likely cationic centers is at the β-position. In previous quantitative structure−activity relationship (QSAR) investigations,[33,34] our results suggested the desirability of increasing charge at this position in order to enhance activity. It might therefore be desirable to introduce a fixed charge at this site, although investigating the effects of varying the number of CH_2 group spacers attached to the bisphosphonate backbone would also seem prudent, since the above discussion does not absolutely rule out optimum activity with a more distal charge center. Of course, the introduction of a fixed charge might further limit the already low bioavailability of a bisphosphonate (as, most likely, with pamidronate and alendronate), although this effect might well be offset by enhanced lipophilicity. And finally, it might be possible to improve activity by varying the actual nature of the side-chain substitution pattern.

We thus decided to synthesize and test three series of compounds containing (1) cyclic sulfonium side chains, (2) aryl-substituted side chains analogous to those reported by Widler et al.,[35] and (3) n-alkyl side chains. The general synthetic routes to produce the sulfonium bisphosphonates were as follows, and full details are given in the Experimental Section.

Dialkyl sulfides reacted smoothly with bromoacetic acid at room-temperature resulting in the corresponding thiobetaine; phosphorylation using $PCl_3-H_3PO_3$−pyridine afforded the β-sulfonium bisphosphonates (Scheme 1). γ-Sulfonium bisphosphonates were produced in a similar manner, except that the carboxylic acid precursors were prepared via addition of alkyl sulfides to acrylic acid (Scheme 2).

The synthesis of deoxy-sulfonium bisphosphonates (lacking the 1-OH group) was achieved in high yield via addition of

Scheme 1[a]

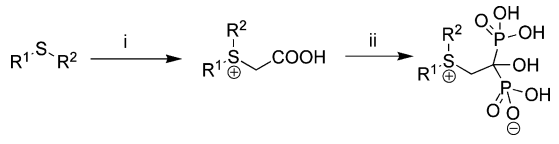

[a] Reagents and conditions: (i) $BrCH_2COOH$, acetone, rt; (ii) PCl_3, H_3PO_3, pyridine-HCl.

Scheme 2[a]

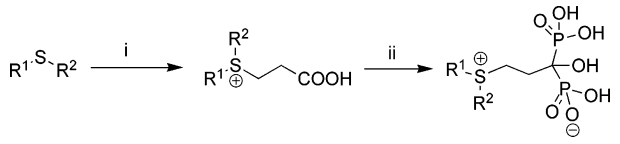

[a] Reagents and conditions: (i) acrylic acid, HCl, acetone, rt; (ii) PCl_3, H_3PO_3, pyridine-HCl.

Scheme 3

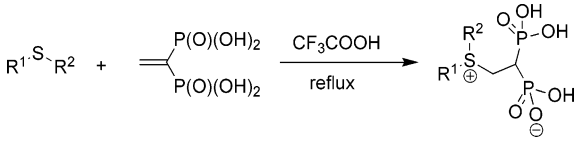

alkyl sulfides to vinylidene-1,1-diphosphonic acid in trifluoroacetic acid (Scheme 3).

Qualitative Structure−Activity Relationship Results. We synthesized 6 thiacycloalkyl, 10 aryl (or aryloxy) alkyl, and 17 n-alkyl bisphosphonates: structures are shown in Figures 1−3, and elemental analysis results are in Supporting Table S1. All compounds were then tested for their ability to inhibit the growth of three tumor cell lines: NCI-H460, MCF-7, and SF-268, and representative growth inhibition results for the most active species in each category are shown in Figure 4A−C (for NCI-H460 cells), together with, for comparison, results for zoledronate (Figure 4D) as a control. On average, the fitted r^2 value (over all compounds and all cell lines) was $r^2 = 0.94$. All IC_{50} values (as well as pIC_{50} values, $pIC_{50} = -\log[IC_{50}\ (M)]$) are shown in Table 1. We find a good correlation between all three data sets with r^2 values of 0.90, 0.94, and 0.98 (shown in the correlation matrix in Figure S1 in the Supporting Information) for MCF-7, NCI-H460, and SF-268. For simplicity, in what follows we discuss, in detail, solely data for NCI-H460, based on the results of the QSAR investigations discussed below, which show that the NCI-H460 predictions are slightly better than those of MCF-7, but worse than SF-268, consistent with the pattern of r^2 values in the experimental results noted above.

(a) Thiacycloalkyl Bisphosphonates. In the first set of compounds, Figure 1, we investigated a series of 6 thiacycloalkyl sulfonium (and one NBP, **47**) bisphosphonates, as exemplified by the most active species, **14,** shown below: The logic here

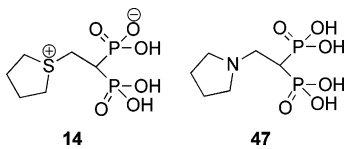

14 **47**

was to try to mimic to some degree the five-membered ring and β-position charge center found in zoledronate. The results obtained with the thiacycloalkyl bisphosphonates showed activity generally similar to that obtained with the second generation, nitrogen-containing bisphosphonates pamidronate and alendronate, with IC_{50} values in the range ~100 to >400 μM, Table 1. The most active compounds contained five-membered rings, although the differences between the five and six ring-atom-containing species were generally small. The presence of an H as opposed to an OH group at C_1 (on the bisphosphonate backbone) appeared to make little difference to activity. The relative lack of activity of these compounds was on the one hand disappointing; however, on the other hand, the observation that the most active compound was about twice as active as pamidronate and alendronate was encouraging since it clearly demonstrates that sulfonium bisphosphonates, containing a cationic center at the β-position, can be quite active and indeed the activity of **14** is some three times greater than that of the analogous NBP **47,** which has an IC_{50} of 294 μM. As can be seen in Table 1 and Figure 1, optimum activity is obtained with a single CH_2-group spacer between the cationic charge center and the bisphosphonate C_1 carbon, with activity falling off upon the addition of more CH_2 groups. For example, in the 1-OH series: $n = 1$, **15**, $IC_{50} = 127$ μM; $n = 2$, **16**, $IC_{50} = 158$ μM; $n = 3$, **19 (**>400 μM**)**, no detectable activity. This result is interesting in that with the nitrogen-containing bisphosphonates, alendronate has $n = 3$ CH_2 groups and is more active (in bone resorption and FPPS inhibition) than is pamidronate ($n = 2$) but is consistent with our previous observation of the importance of a cationic feature at the β-position.[33,34]

(b) Phenylalkyl and Phenyloxyalkyl Bisphosphonates. To try to improve activity, we reasoned that it might be desirable to remove the structural constraints imposed by the ring structure, since it might be that chair/boat or skew boat conformers would be a poor steric match to the FPPS binding site, since they are unlike the planar features found in the most potent bisphosphonates, zoledronate, and minodronate, which are particularly potent FPPS/bone resorption/tumor cell growth inhibitors. However, another series of NBP compounds developed previously by Novartis[35] have almost equipotent activity to that of zoledronate. For example, compound **48** has about

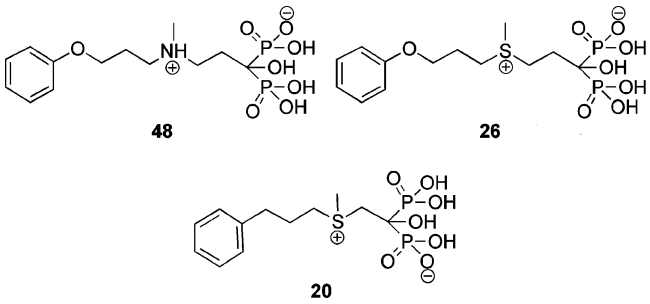

48 **26** **20**

30% the activity of zoledronate,[35] so we reasoned that sulfonium analogues such as **26** (similar in overall length to **15**) might also have good activity. Interestingly, as can be seen in Table 1 (and Figure 2), **26** is actually not the most active species; rather, the compound (**20**) with a single bridging CH_2 group is the most active species. This is the same trend as seen with the thiacycloalkyl species in which **15**, containing a single bridging group, is more active than homologous compounds containing two and three CH_2 backbone spacer groups, consistent again with our previous QSAR observations.[33] The IC_{50} for **20** is ~14 μM, essentially the same as that found for zoledronate (15 μM), an encouraging improvement. More systematically, the activity of **20** decreases from 14 μM to 66 μM on addition of a second CH_2 group (**25**), and the activity of **21** also decreases from 17 μM to 151 μM (**26**) on addition of the second bridging CH_2 group. The presence of an OH group (**24** → **20**) also appears to confer activity in all three tumor cell lines, by a factor of ~3−4. The least active compounds generally contain shorter side chains, with activities in the ~100 μM → ~300 μM range. An

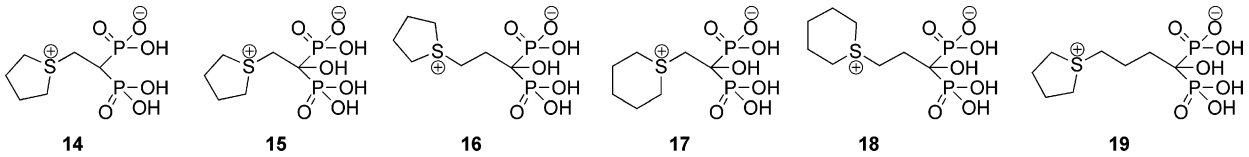

Figure 1. Structures of thiacycloalkyl bisphosphonates, activity decreasing left to right.

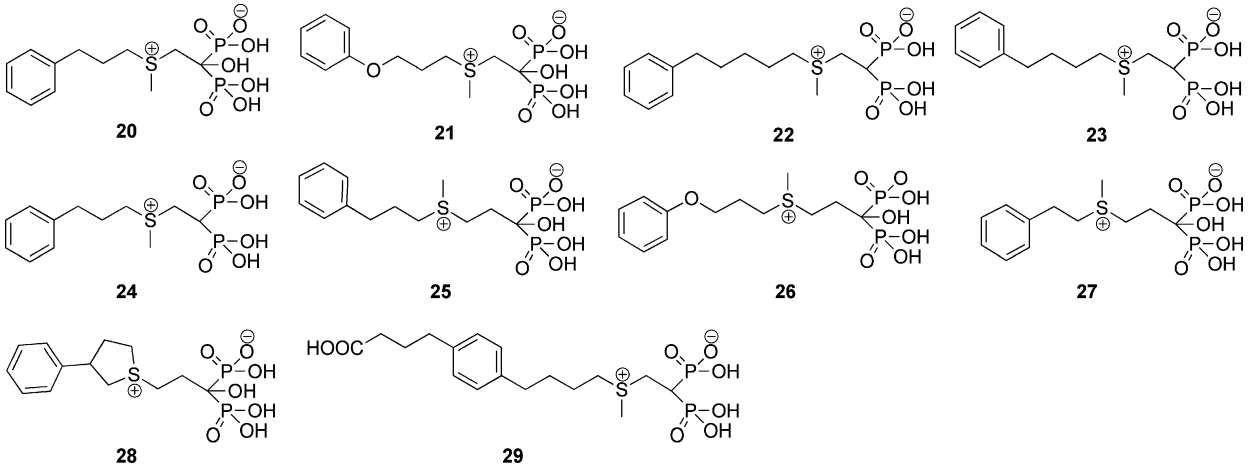

Figure 2. Structures of phenylalkyl and phenyloxyalkyl bisphosphonates, rank ordered by activity.

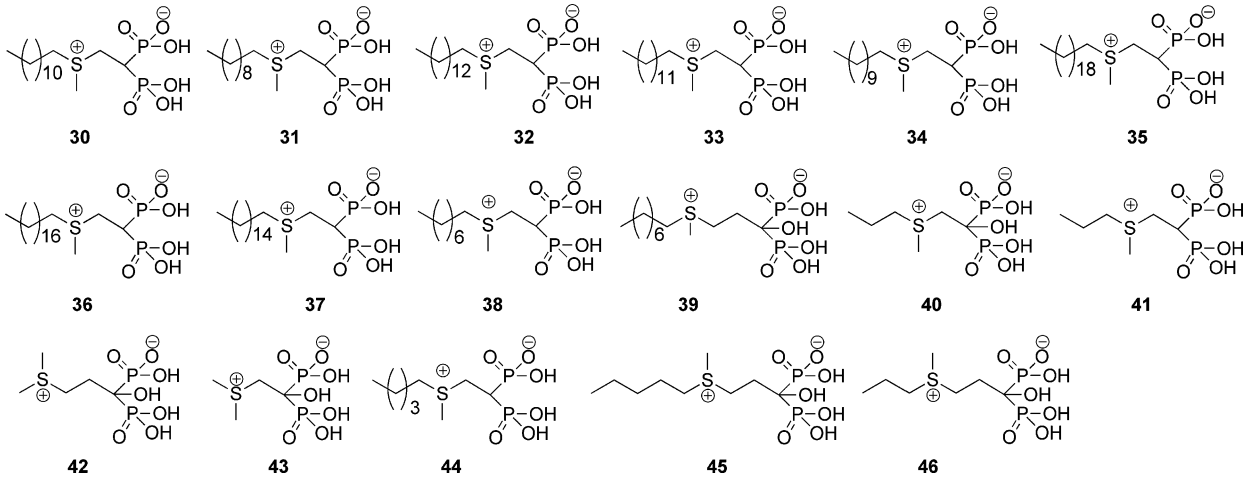

Figure 3. Structures of n-alkylsulfonium bisphosphonates, rank ordered by activity.

exception is that the addition of a polar moiety to the aryl group (an attempt to design a compound which might bind to His93 in the active site of *T. brucei* FPPS) also abrogated activity, presumably because of unfavorable interactions with more hydrophobic active site residues.

The activities of the compounds having the cationic center in the β-position and with longer side chains are all in the 50 μM range, and the two most active species have activities of $\sim$14 μM (**20**) and $\sim$17 μM (**21**), about the same as zoledronate. This encouraged us to further investigate the effects of chain length on activity, focusing on n-alkyl sulfonium species, since these are very readily prepared from commercially available materials and provide a simple method with which to deduce the optimum overall chain length.

(c) n-Alkylsulfonium Bisphosphonates. We prepared a series of n-alkylsulfonium bisphosphonates (Figure 3) and determined their activities in tumor cell growth inhibition (Table 1). The most active compound (**30**) (NCI-H460) had an IC_{50} of 210 nM, a factor of $\sim$70$\times$ more active than zoledronate. All of the most active n-alkyl sulfonium bisphosphonates (IC_{50} $\sim$200 nM to 8 μM) contained a single CH_2 group spacer, the most active dimethylene group-containing species (**42**) having an IC_{50} of $\sim$95 μM (Table 1), basically the same pattern of activity observed for the phenyl-containing species described above.

Quantitative Structure−Activity Relationships. On the basis of the results discussed above, it seemed clear that there is a relationship between the activity and the overall length of the inhibitor, shown graphically in Figure 4E in which we plot pIC_{50} as a function of the molecular diameter[36] for all molecules investigated (Figures 1−3). Tumor cell growth inhibition is maximal with a $\sim$15 Å chain length. We see the same trend when plotting the FPPS pIC_{50} against molecular diameter (Figure 4F, Supporting Table S2). This is not unexpected, since FPPS is a known target for bisphosphonates and likely a major target for sulfonium bisphosphonates. To obtain a more pictorial view of the results discussed above, we produced a common feature pharmacophore model using the Molecular Operating Environment (MOE)[37] program. The pharmacophore (Figure 5) shows the importance of distal hydrophobic (green) and aromatic (pink) features, together with a cationic (blue) feature, centered as anticipated on the β position, in addition to the presence of two acceptor/anionic/metal binding sites, the bisphosphonate backbone (yellow, Figure 5). These observations correlate well with the features noted previously, but based on

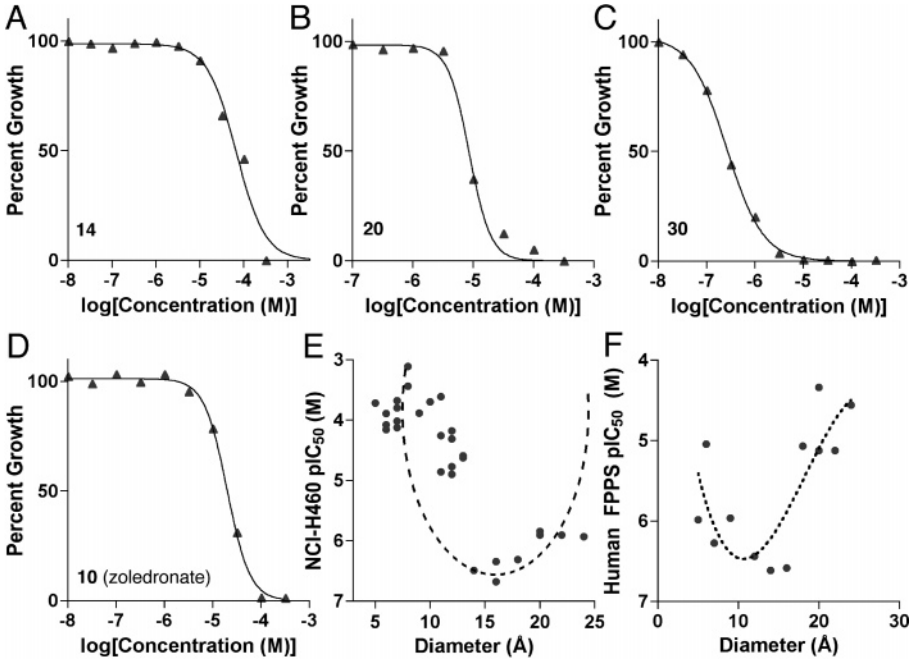

Figure 4. Representative dose−response curves and molecular diameter−activity scatter plots. (A−D) Dose response curve fitting for most active compounds from each group: (A) **14**, 80 μM; (B) **20**, 9.4 μM; (C) **30**, 262 nM; (D) zoledronate control, 15 μM. (E) Tumor cell growth inhibition activity as a function of molecular diameter; most active compounds are ~15 Å long. (F) FPPS inhibition as a function of molecular diameter; most active compounds again have a ~15 Å length (dotted lines are to "guide the eye").

Table 1. Tumor Cell Growth Inhibition by Sulfonium Bisphosphonates

class	compd[a]	NCI-H460 IC_{50} (μM)	activity MCF-7 IC_{50} (μM)	SF-268 IC_{50} (μM)
thiacycloalkyl	**14**	82.7	96	87.8
	15[b]	127	89.1	101
	16[b]	158	197	129
	17[b]	207	304	240
	18[b]	359	517	431
	19	>400 mM	>400 mM	>400 mM
phenylalkyl and phenyloxyalkyl-sulfonium	**20**	13.7	17.7	10.7
	21	16.8	94.2	34.5
	22	23.5	21.2	17.9
	23	48.1	45.5	43.9
	24	54.4	58.1	48.6
	25	65.8	106	65.9
	26	151	184	171
	27	183	251	198
	28[b]	243	337	264
	29	>400 mM	>400 mM	>400 mM
n-alkylsulfonium	**30**	0.21	0.24	0.29
	31	0.32	0.62	0.37
	32	0.48	10.9	0.88
	33	3.4	2.8	3.1
	34	3.7	14.2	3.7
	35	1.15	0.96	1.49
	36	1.23	1.43	1.71
	37	1.41	1.12	1.08
	38	12.4	21.3	14.7
	39	25.5	32	20.3
	40	74.6	161	96.1
	41[b]	94.6	241	223
	42[b]	95.1	258	100
	43	189	199	171
	44	128	224	189
	45[b]	197	386	196
	46[b]	759	815	714

[a] Structures shown in Figures 1−3. [b] Highest concentration tested, 5 mM.

our previous work, was not expected to provide a highly predictive model. We thus next consider three QSAR modeling approaches.

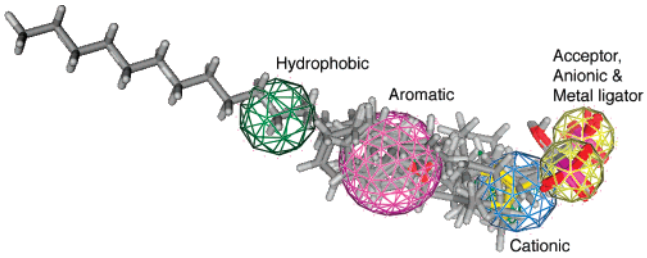

Figure 5. Common feature pharmacophore. Pharmacophore features are superimposed on the alignment of all sulfonium species. Yellow sphere, combined feature of acceptor, anion, and metal ligator; blue sphere, cation; green spheres, hydrophobic; magenta sphere, aromatic.

In the first, we constructed a molecular descriptor-based model using the program MOE[37] in combination with the AutoQuaSAR[38] module. To provide sufficient granularity, subdivided van der Waals surface area descriptors[39] (as implemented in MOE) were utilized in the molar refractivity and positive charge terms, as opposed to whole molecule-based descriptors (see Supporting Methods for full details). The final cross-validated (NCI-H460) model yielded $r^2 = 0.84$, $q^2 = 0.77$, $F = 74.3$, $n = 25$. Training and test set predictions are shown in Figure 6A and Table 2, with similar results for SF-268 and MCF-7 shown in the Supporting Figure S2 and Tables S3−S7. A second analysis was performed using the HQSAR[40] module in Sybyl 7.3. In this method, molecular holograms (fingerprints) were used to encode structural information about each molecule. These holograms were then utilized by a PLS algorithm within Sybyl to produce a linear model, yielding $r^2 = 0.76$ and $q^2 = 0.635$, Figure 6B and Supporting Figure S3 and Table S8.

Of course, while these statistics are not wholly unreasonable, it is obvious from the results shown in Figure 6A,B that these linear models are oversimplified. More specifically, they predict that the longer chain species (**30** and **31**) are less active than they actually are; plus they overestimate the activity of the shorter chain and phenylalkyl species (**24**, **23**, **46**). We therefore next used the comparative molecular similarity analysis (CoM-

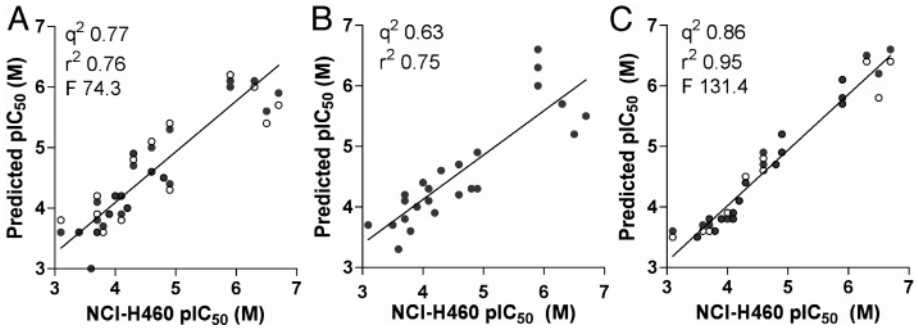

Figure 6. Molecular descriptor, HQSAR, and CoMSIA results. (A) Molecular descriptor QSAR based on 2D and 3D alignment independent descriptors showing $q^2 = 0.77$, $r^2 = 0.76$. Test and training set shown, training = ●, test = ○. (B) Hologram QSAR results based on 2D connectivity information, $q^2 = 0.63$, $r^2 = 0.75$. (C) CoMSIA modeling results for NCI-H460 cell line and feature-based alignment, $q^2 = 0.86$, $r^2 = 0.95$, test and training shown, training = ●, test = ○.

Table 2. Molecular Descriptor QSAR Results for NCI-H460 Tumor Cell Line.

compd[a]	contiguous rotatable bonds	Weiner path	molar refractivity (SMR VSA7)	Gasteiger charge (VSA+2)	NCI-H460 pIC_{50} (M)	predicted pIC_{50} (M)	CV predicted[b] pIC_{50} (M)	residual
30	14	1818	110.91148	12.37335	6.7	5.9	5.7	1
31	12	1353	110.91148	12.37335	6.5	5.6	5.4	1.1
32	16	2379	110.91148	12.37335	6.3	6.1	6	0.3
35	22	4718	110.91148	12.37335	5.9	6	6.2	−0.2
37	18	3044	110.91148	12.37335	5.9	6.1	6.2	−0.4
36	20	3821	110.91148	12.37335	5.9	6.1	6.2	−0.3
20	6	1154	77.585464	10.677375	4.9	4.4	4.3	0.6
38	10	976	110.91148	12.37335	4.9	5.3	5.4	−0.5
21	7	1360	77.585464	10.677375	4.8	4.5	4.5	0.3
22	9	1464	77.585464	12.37335	4.6	5	5.1	−0.4
39	10	1261	110.91148	30.056063	4.6	4.6	4.6	0
23	8	1249	77.585464	12.37335	4.3	4.9	4.9	−0.6
24	7	1056	77.585464	12.37335	4.3	4.7	4.8	−0.5
25	7	1362	77.585464	30.056063	4.2	4	4	0.2
14	3	351	45.894287	23.050724	4.1	4.2	4.2	−0.2
40	4	413	110.91148	10.677375	4.1	3.9	3.8	0.3
41	5	366	110.91148	12.37335	4	4.2	4.2	−0.2
15	2	397	45.894287	21.35475	3.9	3.9	3.9	0
16	3	499	45.894287	40.733437	3.8	3.7	3.6	0.2
43	2	270	109.27663	0	3.7	3.6	3.6	0.2
17	2	478	45.894287	21.35475	3.7	3.8	3.9	−0.2
45	7	756	110.91148	30.056063	3.7	4.1	4.2	−0.5
28	3	1129	58.534134	40.733437	3.6	3	2.6	1
18	3	595	45.894287	40.733437	3.4	3.6	3.6	−0.2
46	5	516	110.91148	30.056063	3.1	3.6	3.8	−0.7

[a] Structures shown in Figures 1−3. [b] Predicted values obtained from leave-one-out cross validation.

SIA) method to more explicitly model three-dimensional structural information (Table 3). For CoMSIA, we used two sets of alignments, and partial least-squares (PLS) to regress against cell activity and field data. In the first alignment, we used the maximum common substructure (MCS) alignment, and in the second, we used an alignment constructed in the flexible alignment module[41] of MOE, which perceives common features within the ligands (e.g., similar charge, hydrophobic area, volume, etc.). In both cases, we used fully deprotonated bisphosphonate groups, based on the results of ^{31}P NMR chemical shift and quantum chemical calculations reported previously,[28] and the observation that bisphosphonates bind three Mg^{2+} in the FPPS active site.[25−29] For alignment 1 (MCS, Figure 7A), we obtained: q^2 (no. of components), r^2, *F*-test, pIC_{50} error values of 0.819 (4), 0.94, 80.18, 0.27 for NCI-H460; 0.61 (4), 0.91, 51.7, 0.33 for MCF-7; and 0.80 (4), 0.94, 79.0, 0.27 for SF-268. Interestingly, we observed better performance from the feature-based alignment (Figure 7B), with q^2 (no. of components), r^2, *F*-test, error values of: 0.86 (4), 0.96, 131, 0.216 for NCI-H460; 0.73 (4), 0.93, 61.8, 0.30 for MCF-7; and 0.85 (4), 0.96, 118, 0.22 for SF-268. We then performed five iterations of a leave-two-out test/training set approach, observing (on average for the feature alignment) a factor of 1.7× error between predicted and experimental IC_{50} values in three cell lines. Training and test set predictions are shown in Figure 6C and Supporting Figure S4 with full details of the CoMSIA descriptors given in the Supporting Information (Tables S9−S13). Selected CoMSIA fields (for the NCI-H460 models, both alignments) are shown in Figure 7C−F. Both sets of fields were generally consistent, particularly in the steric (green, Figure 7C,D) and hydrophobic-favorable regions (yellow, Figure 7E,F). In the MCS alignment, Figure 7C, a steric penalty feature (yellow) near the location of the thiacycloalkyl ring, and additionally, a hydrophobic penalty near the OH group at the Cα position were observed, consistent with the experimental activities seen: reduced activity beyond an optimum chain length (∼15 Å), reduced activity for thiacycloalkyl species versus n-alkyl, and the overall most active compounds lack the backbone OH group. A comparison of the experimental results and computational predictions for each alignment and dataset are shown graphically in Supporting Figure S1.

For further validation, a stability test was performed using the progressive scrambling module[42] in Sybyl 7.11, which applies small, random perturbations to the activity data of structurally similar compounds, allowing determination of the sensitivity of a PLS model to these small systematic perturba-

Table 3. CoMSIA Results for NCI-H460 Tumor Cell Line Using the Feature Alignment

	NCI-H460 experimental activity		CoMSIA pIC_{50} predictions							
				test sets[b]						
compd[a]	IC_{50} (μM)	pIC_{50} (M)	training set	1	2	3	4	5	pred	residual
30	0.21	6.7	6.6	6.7	6.7	6.4	6.4	6.7	6.4	−0.28
31	0.32	6.5	6.2	6.2	6.2	5.8	6.1	6.2	5.8	−0.70
32	0.48	6.3	6.5	6.4	6.5	6.4	6.3	6.6	6.4	0.13
35	1.15	5.9	5.7	5.7	5.6	5.7	5.7	5.7	5.7	−0.24
36	1.23	5.9	5.8	5.8	5.8	5.8	5.8	5.9	5.8	−0.07
37	1.41	5.9	6.1	**6.1**	6.1	6.1	6.1	6.2	6.1	0.25
38	12.30	4.9	5.2	5.2	5.2	5.1	5.3	5.2	5.2	0.27
20	13.80	4.9	4.9	4.9	4.9	4.9	4.9	4.9	4.9	0.05
21	16.60	4.8	4.7	4.7	4.6	4.5	**4.7**	4.7	4.7	−0.08
22	23.44	4.6	4.9	4.8	**4.8**	4.8	5.2	4.8	4.8	0.17
39	25.70	4.6	4.7	4.7	4.4	4.6	4.8	4.6	4.6	0.03
23	47.86	4.3	4.4	4.3	4.4	4.4	4.4	4.4	4.4	0.09
24	54.95	4.3	4.4	4.3	4.4	**4.5**	4.5	4.4	4.5	0.24
25	66.07	4.2	4.1	4.1	4.1	4.1	4.1	4.1	4.1	−0.08
40	74.13	4.1	3.9	3.9	3.8	3.9	3.9	3.9	3.9	−0.26
14	83.18	4.1	3.8	3.7	3.8	3.8	3.8	3.8	3.8	−0.26
41	95.50	4.0	3.8	3.8	**3.9**	3.9	3.9	3.9	3.9	−0.12
15	125.89	3.9	3.8	3.7	3.8	3.8	3.7	3.8	3.8	−0.14
16	158.49	3.8	3.6	3.6	3.6	3.5	3.6	3.6	3.6	−0.25
43	190.55	3.7	3.8	**3.8**	3.7	3.7	3.8	3.8	3.8	0.08
45	199.53	3.7	3.7	3.6	3.6	3.6	3.6	3.6	3.6	−0.08
17	208.93	3.7	3.8	3.8	3.8	3.9	3.8	3.9	3.8	0.16
28	245.47	3.6	3.7	3.7	3.7	3.6	3.6	**3.6**	3.6	−0.01
18	354.81	3.5	3.5	3.5	3.5	3.5	3.5	3.5	3.5	0.06
46	758.58	3.1	3.6	3.6	3.5	3.5	3.6	3.5	3.5	0.42
		q^2	0.86	0.83	0.86	0.83	0.79	0.84		
		R^2	0.96	0.96	0.96	0.96	0.95	0.96		
		F test	131.4	117.6	140.9	113.1	91.74	120.9		
		N	4	4	4	4	4	4		
		n	25	23	23	23	23	23		

[a] Structures shown in Figures 1−3. [b] Bold values represent predicted activities of compounds that were not included in the training set.

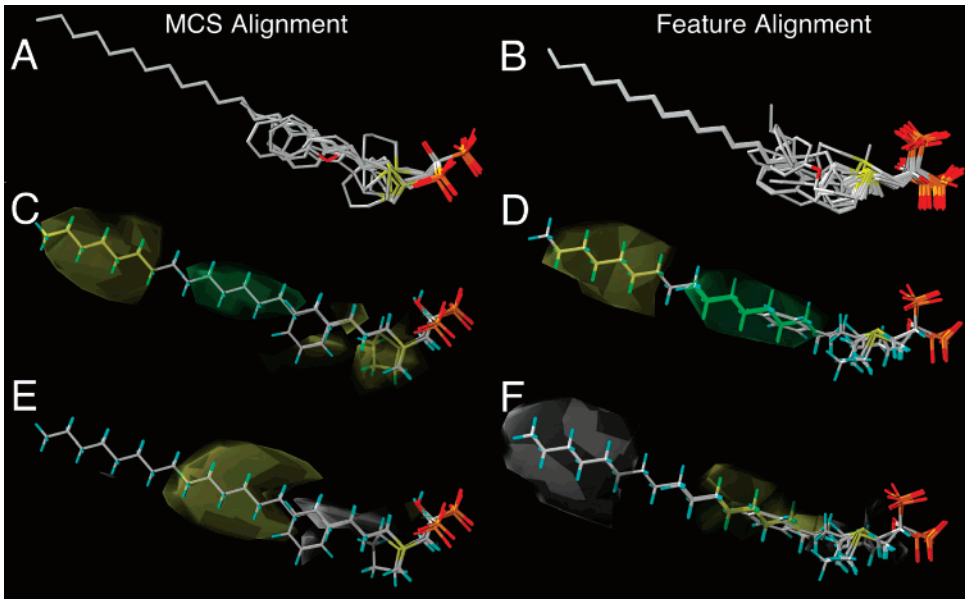

Figure 7. Representative CoMSIA fields for MCS and feature-based alignments (NCI-H460 model). (A, C, E) MCS alignment and fields: (A) MCS alignment, only heavy atoms displayed for clarity; (C) steric fields, green favorable, yellow disfavored; (E) hydrophobic fields, yellow favored, gray disfavored. (B, D, F) feature-based alignment and fields; (B) feature-based alignment, only heavy atoms displayed for clarity; (D) steric fields, green favorable, yellow disfavored; (F) hydrophobic fields, yellow favored, gray disfavored.

tions.[43] The analysis yielded an effective slope of 1.1 for NCI-H460 (MCF-7 = 0.91, SF-268 = 1.1), close to the ideal value of 1, indicating good stability. Data randomization was also performed to check that a model could not be the result of a chance correlation. The randomization tests produced no usable models (q^2 < 0.1) among 10 iterations for each alignment.

Sulfonium Bisphosphonate−FPPS Interactions. The results discussed above are of general interest since we have produced numerous bisphosphonates that, at least in cell growth inhibition assays, are very active. This, of course, then leads to the question as to how they might bind to their FPPS target. To answer this question, we elected to determine the single-crystal X-ray crystallographic structure of the simplest bisphosphonate, **43**,

Table 4. Data Collection and Refinement Statistics for **15**[a] Bound to Human FPPS and *T. Brucei* FPPS (PDB: 2OPN, 2OGD)

crystals	**15**[a] + human FPPS	**15**[a] + *T. brucei* FPPS
	Data Collection	
space group	$P4_12_12$	$C2$
unit cell dimension (Å)		
a, *b*, *c*	111.65, 111.65, 66.84	134.61, 118.37, 62.76
α, *β*, *γ* (°)	90, 90, 90	90, 112.158, 90
X-ray source	BNL-X29[b]	BNL-X8C[b]
wavelength (Å)	0.9791	1.1
resolution (Å)[c]	30-2.70 (2.80-2.70)	30-2.00 (2.07-2.00)
no. of reflections obsd	135,612	461,159
unique	12,031 (1,154)	61,155 (6,046)
completeness (%)	99.0 (97.7)	99.8 (99.5)
R-merge	0.107 (0.384)	0.082 (0.538)
$I/\sigma I$	30.0	33.6
multiplicity	11.3 (8.4)	7.5 (7.4)
	Refinement Statistics	
resolution range (Å)	30.0-2.70	30.0-2.00
R-work/*R*-free (%)	27.24/29.79	20.70/24.12
RMSD		
bond lengths	0.004	0.008
bond angles	1.414	1.21
no. of atoms		
protein	2,664	5,715
ligand	14	28
magnesium ion	3	6
solvent (water)	98	563
B average (Å^2) of protein	48.9	28.4
B average (Å^2) of solvents	55.2	36.1
B average (Å^2) of ligands (bisphosphonates, Mg^{2+}, and PO_4^{3-})	67.6	22.9

[a] **15** is 2-hydroxy-2,2-bis-phosphonoethyl)dimethylsulfonium. [b] Brookhaven National Laboratory. [c] Values in the parentheses are for the highest resolution shell.

bound to human and *T. brucei* FPPS, the latter being of interest as a target for antiinfective therapy. We anticipated, based on the transition state/reactive intermediate model described above, that this bisphosphonate would bind to the allylic binding site and chelate to Mg^{2+}, although given its small size, binding to the IPP binding site would be hard to exclude. Bisphosphonate **43** has a 1 μM IC_{50} versus human FPPS (Table S2) and an IC_{50} in cell growth inhibition of ~190 μM, to be compared (in the same assay) with a 0.12 μM FPPS IC_{50} for zoledronate, which as noted above, has a 15 μM value in cell growth inhibition. The activity of **43** is, therefore, basically similar to that of second-generation bisphosphonates, such as pamidronate. Full details of protein expression, purification, and crystallization were as described previously,[28,44] and X-ray crystallographic data collection and refinement statistics are given in Table 4. **43** binds to the allylic or DMAPP site in both human and *T. brucei* FPPS, the latter structure having improved resolution over that of the human FPPS, 2.07 Å versus 2.80 Å. The two phosphonate groups interact with three Mg^{2+}, Figure 8A,B, as reported previously for many nitrogen-containing bisphosphonates.[25−28] Also of interest is the observation that the (cationic) sulfonium charge center is in essentially the same location as is N_1 (the β-position) in zoledronate, bound to human FPPS, shown superimposed on **43** in Figure 8B. To see if this binding pose might be predicted computationally, we used the Glide[45] program to dock **43** to the human and *T. brucei* structures determined here (PDB: 2OPN, 2OGD) and to one other structure, of **48** bound to *T. brucei* FPPS (PDB: 2PlC), in each case, minus the bisphosphonate ligand. For the six pairwise experimental/predicted structure comparisons (two experimental structures, three predicted poses) there was a 1.0 ± 0.19 Å rmsd between the experimental and predicted ligand heavy atom positions, and one such comparison is shown in Figure 8C. This gave some confidence in the method, so we next docked the most active species in each of the three classes of compounds (**14**, **20**, and **30**) to the **43** human FPPS structure (PDB: 2OPN, minus the bisphosphonate ligand). The results obtained are shown in Figures 8D−F and indicate that, in each case, the bisphosphonate moiety binds to the $3Mg^{2+}$ cluster, while the large side chains bind in the hydrophobic central channel in the protein. For the phenylalkyl species, this binding pattern is very similar to that seen crystallographically with **15** bound to *T. brucei* FPPS (PDB: 2PlC), giving further confidence in the predictions for the other compounds. Of course, on the basis of these results alone, we cannot definitely state that FPPS is the sole target for, in particular, the n-alkyl bisphosphonates, where geranylgeranyl diphosphate synthase might also be targeted. However, the most active n-alkyl bisphosphonate (**30**) does have an IC_{50} of 0.26 μM against human FPPS (Table S2), supporting FPPS as a "primary" target for these types of compounds.

Experimental Section

Synthetic Aspects. All reagents used were purchased from Aldrich (Milwaukee, WI). The purities of all compounds produced were routinely monitored by using ^1H and ^{31}P NMR spectroscopy at 400 or 500 MHz on Varian (Palo Alto, CA) Unity spectrometers. In some instances, absolute spin-count quantitative analyses using an internal imidazole standard were performed. The elemental analysis results for all new compounds are provided in the Supporting Information (Table S1).

General Method A: Synthesis of 2-(Sulfonium-1-yl)acetic Acid. A mixture of alkyl sulfide (1 mmol) and bromoacetic acid (1.2 mmol) was stirred in anhydrous acetone (2 mL) under N_2 at room temperature overnight. The precipitate was washed with ether and dried under vacuum to afford 2-(sulfonium-1-yl)acetic acid as a white powder.

General Method B: Synthesis of 3-(Sulfonium-1-yl)propanoic Acid. Concentrated HCl (2 mL) was added to a mixture of alkyl sulfide (10 mmol) and acrylic acid (10 mmol) in acetone (5 mL) at 0 °C. The mixture was allowed to rise to room temperature and stirred overnight. Upon evaporation of solvent, the residue was

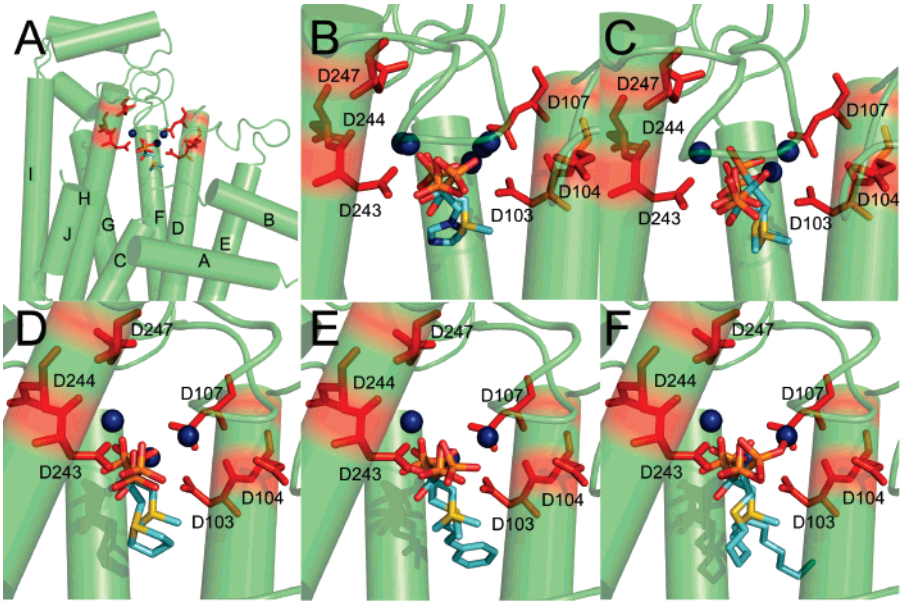

Figure 8. X-ray and docking results. (A) **43** bound to the allylic or DMAPP binding site of human FPPS (PDB: 2OPN)**;** (B) **43** (from human FPPS, PDB: 2OPN) structure superimposed on the zoledronate-FPPS structure (PDB: 1ZW5); (C) Docked pose of **43** obtained using Glide superimposed onto **43** in human FPPS (PDB: 2OPN); (D−F) Docked poses of most active compounds from each category, neighboring Asp residues labeled for clarity; (D) **14**; (E) **20**; (F) **30**.

washed with ethyl acetate (2 × 5 mL) and then dried under vacuum to afford the 3-(sulfonium-1-yl)propanoic acid as a syrup or white powder.

General Method C: Synthesis of Sulfonium Bisphosphonate from a Carboxylic Acid. A mixture of sulfonium carboxylic acid (10 mmol), H_3PO_3 (40 mmol), and pyridine-HCl (30 mmol) was heated to 70 °C and melted. PCl_3 (40 mmol) was added slowly and the reaction mixture stirred at 70 °C for 4 h. H_2O (5 mL) was then cautiously added and the mixture refluxed for 1 h. Upon filtration and evaporation, the residue was precipitated with 2-propanol, washed with acetone (5 × 5 mL), dried, and then further purified by recrystallization from H_2O/*i*-PrOH. In some cases, the bisphosphonate was neutralized with NaOH and crystallized as the sodium salt from H_2O/EtOH.

General Method D: Syntheis of Deoxy-sulfonium Bisphosphonates (Scheme 3). A substituted sulfide (1.2 mmol) and vinylidene-1,1-bisphosphonic acid (1 mmol) was refluxed overnight in trifluoroacetic acid (3 mL). Upon removal of solvent, the residue was triturated with acetone (3 mL), and the resulting white suspension filtered and washed with acetone (2 × 2 mL), affording pure 2-(sulfonium-1-yl)ethylidene-1,1-bisphosphonic acid as a white powder.

2-(Tetrahydrothiophenyium-1-yl)ethylidene-1,1-bisphosphonic Acid (14). Compound **14** was prepared from tetrahydrothiophene (210 mg, 2.4 mmol) and vinylidene-1,1-diphosphonic acid (380 mg, 2 mmol) following General Method D (420 mg, 1.50 mmol, 75%). Anal. ($C_6H_{14}O_6P_2S$·0.25H_2O) C, H. ^{1}H NMR (400 MHz, D_2O): δ 3.20−3.42 (m, 4H), 2.00−2.35 (m, 5H). ^{31}P NMR (D_2O): δ 14.73.

1-Hydroxy-2-(tetrahydrothiophenyium-1-yl)ethylidene-1,1-bisphosphonic Acid (15). Compound **15** was prepared from tetrahydrothiophene (880 mg, 10 mmol) following General Methods A and C (780 mg, 2.7 mmol, 27%). Anal. ($C_6H_{14}O_7P_2S$) C, H. ^{1}H NMR (400 MHz, D_2O): δ 3.20−3.42 (m, 4H), 2.00−2.35 (m, 5H). ^{31}P NMR (D_2O): δ 15.01.

1-Hydroxy-3-(tetrahydrothiophenyium-1-yl)propylidene-1,1-bisphosphonic Acid (16). Compound **16** was prepared from tetrahydrothiophene (880 mg, 10 mmol) following General Methods B and C (460 mg, 1.5 mmol, 15%). Anal. ($C_7H_{16}O_7P_2S$·0.25H_2O) C, H. ^{1}H NMR (400 MHz, D_2O): δ 3.00−3.48 (m, 4H), 1.88−2.15 (m, 4H). ^{31}P NMR (D_2O): δ 18.01.

1-Hydroxy-3-(tetrahydrothiopyranium-1-yl)ethylidene-1,1-bisphosphonic Acid (17). Compound **17** was prepared from tetrahydrothiopyran (1.02 g, 10 mmol) following General Methods A and C (673 mg, 2.2 mmol, 22%). Anal. ($C_7H_{16}O_7P_2S$) C, H. ^{1}H NMR (400 MHz, D_2O): δ 3.40−3.48 (m, 2H), 3.27−3.38 (m, 2H), 1.92−2.05 (m, 2H), 1.60−1.80 (m, 2H), 1.4−1.6 (dm, 2H, J = 6.5 Hz). ^{31}P NMR (D_2O): δ 15.50.

1-Hydroxy-3-(tetrahydrothiopyranium-1-yl)propylidene-1,1-bisphosphonic Acid (18). Compound **18** was prepared from tetrahydrothiopyran (1.02 g, 10 mmol) following General Methods B and C (560 mg, 1.7 mmol, 17%). Anal. ($C_8H_{18}O_7P_2S$·0.5H_2O) C, H. ^{1}H NMR (400 MHz, D_2O): δ 3.40−3.48 (m, 2H), 3.27−3.38 (m, 2H), 2.1−2.22 (m, 2H), 1.92−2.05 (m, 2H), 1.60−1.75 (m, 2H), 1.4−1.6 (dm, 2H, J = 6.5 Hz). ^{31}P NMR (D_2O): δ 17.80.

1-Hydroxy-4-(tetrahydrothiophenyium-1-yl)butylidene-1,1-bisphosphonic Acid (19). Compound **19** was prepared from 1-(3-carboxypropyl)tetrahydrothiophenium bromide (1.0 g, 3.9 mmol) following General Method C (357 mg, 1.1 mmol, 28%). Anal. ($C_8H_{18}O_7P_2S$·0.4H_2O) C, H. ^{1}H NMR (400 MHz, D_2O): δ 3.30−3.42 (m, 2H), 3.18−3.28 (m, 2H), 3.00−3.10 (m, 2H), 2.0−2.2 (m, 4H), 1.75−1.98 (m, 4H). ^{31}P NMR (D_2O): δ 19.88.

1-Hydroxy-2-(phenylpropyl, methyl sulfonium-1-yl)propylidene-1,1-bisphosphonic Acid (20). Compound **20** was prepared from methyl phenylpropyl sulfide (500 mg, 3.01 mmol) following General Methods A and C (136 mg, 0.36 mmol, 12%). Anal. ($C_{12}H_{20}O_7P_2S$·0.4H_2O). ^{1}H NMR (400 MHz, D_2O): δ 7.05−7.20 (m, 5H), 3.41−3.65 (m, 2H), 3.0−3.11 (m, 1H), 3.15−3.24 (m, 1H), 2.75 (s, 3H), 2.60 (t, J = 7.5 Hz), (1.85−2.00) (m, 2H). ^{31}P NMR (D_2O): δ 18.00.

1-Hydroxy-2-(methyl, 3-phenyloxypropylsulfonium-1-yl)ethylidene-1,1-bisphosphonic Acid (21). Compound **21** was prepared from methyl 3-phenyloxypropyl sulfide (1.1 g, 6 mmol) following General Methods A and C (358 mg, 9 mmol, 15%). Anal. ($C_{12}H_{20}O_8P_2S$·0.5H_2O) C, H. ^{1}H NMR (400 MHz, D_2O): δ 7.18 (t, J = 7.5 Hz, 2H), 6.85−6.90 (m, 3H), 4.04 (t, J = 6 Hz, 2H), 3.50−3.70 (m, 2H), 3.18−3.40 (m, 2H), 2.75 (s, 3H), 2.02−2.15 (m, 2H). ^{31}P NMR (D_2O): δ 15.30.

2-(Methyl, phenypentylsulfonium-1-yl)ethylidene-1,1-bisphosphonic Acid (22). Compound **22** was prepared from methyl phenylpentyl sulfide (466 mg, 2.4 mmol) and vinylidene-1,1-diphosphonic acid (380 mg, 2 mmol) following General Method D (453 mg, 1.16 mmol, 58%). Anal. ($C_{14}H_{24}O_6P_2S$·0.5H_2O) C, H. ^{1}H NMR (400 MHz, D_2O): δ 7.00−7.21 (m, 5H), 3.20−3.35 (m, 2H), 3.10−3.20 (m, 1H), 2.95−3.00 (m, 1H), 2.90−3.00 (m, 1H), 2.63 (s, 3H), 2.5−2.60 (t, J = 7.5 Hz, 2H), 1.90−2.05 (m, 1H),

1.60−1.70 (m, 2H), 1.41−1.55 (m, 2H), 1.20−1.35 (m, 2H). ^{31}P NMR (D_2O): δ 15.01 (d, J = 17.4 Hz).

2-(Methyl, phenylbutylsulfonium-1-yl)ethylidene-1,1-bisphosphonic Acid (23). Compound **23** was prepared from methyl phenylbutyl sulfide (466 mg, 2.4 mmol) and vinylidene-1,1-diphosphonic acid (380 mg, 2 mmol) following General Method D (524 mg, 1.4 mmol, 70%). Anal. ($C_{13}H_{22}O_6P_2S\cdot0.3H_2O$) C, H. ^{1}H NMR (400 MHz, D_2O): δ 7.00−7.22 (m, 5H), 3.20−3.40 (m, 2H), 3.10−3.20 (m, 1H), 2.95−3.00 (m, 1H), 2.90−3.00 (m, 1H), 2.63 (s, 3H), 2.5−2.60 (t, J = 7.5 Hz, 2H), 1.90−2.05 (m, 1H), 1.60−1.70 (m, 4H). ^{31}P NMR (D_2O): δ 15.01 (d, J = 16.8 Hz).

2-(Methyl, phenylpropylsulfonium-1-yl)ethylidene-1,1-bisphosphonic Acid (24). Compound **24** was prepared from methyl phenylpropyl methyl sulfide (400 mg, 2.4 mmol) and vinylidene-1,1-diphosphonic acid (380 mg, 2 mmol) following General Method D (414 mg, 1.14 mmol, 57%). Anal. ($C_{12}H_{20}O_6P_2S\cdot0.5H_2O$) C, H. ^{1}H NMR (400 MHz, D_2O): δ 7.01−7.25 (m, 5H), 3.27−3.53 (m, 2H), 3.13−5-3.20 (m, 1H), 2.90−3.03 (m, 1H), 2.61 (s, 3H), 1.95 (t, J = 7.5 Hz, 2H). ^{31}P NMR (D_2O): δ 15.18.

1-Hydroxy-3-(phenylpropyl, methylsulfonium-1-yl)propylidene-1,1-bisphosphonic Acid (25). Compound **25** was prepared from phenylpropyl sulfide (1.0 g, 6 mmol) following General Methods B and C (283 mg, 0.72 mmol, 12%). Anal. ($C_{13}H_{22}O_7P_2S\cdot0.5H_2O$). ^{1}H NMR (400 MHz, D_2O): δ 7.10−7.25 (m, 5H), 2.95−3.51 (m, 4H), 2.7−2.90 (m, 5H), 2.0−2.22 (m, 2H), 1.70−1.95 (m, 2H). ^{31}P NMR (D_2O): δ 18.00.

1-Hydroxy-3-(methyl, phenyloxypropylsulfonium-1-yl)propylidene-1,1-bisphosphonic Acid (26). Compound **26** was prepared from methyl phenyloxypropyl sulfide (0.6 g, 3.3 mmol) following General Methods B and C. (189 mg, 0.43 mmol, 13%). Anal. ($C_{13}H_{13}NaO_9P_2S$) C, H, N. ^{1}H NMR (400 MHz, D_2O): δ 6.8−7.2 (m, 5H), 4.04 (t, J = 6 Hz, 2H), 3.50−3.70 (m, 2H), 3.18−3.40 (m, 2H), 2.72 (s, 3H), 2.2−2.3 (m, 2H). ^{31}P NMR (D_2O): δ 17.89.

1-Hydroxy-3-(phenylethyl, methylsulfonium-1-yl)propylidene-1,1-bisphosphonic Acid (27). Compound **27** was prepared from methyl phenylethyl sulfide (0.69 g, 4.5 mmol) following General Methods B and C (166 mg, 0.405 mmol, 9%). Anal. ($C_{12}H_{19}NaO_7P_2S\cdot1.3H_2O$). ^{1}H NMR (400 MHz, D_2O): δ 7.15−7.27 (m, 5H), 3.30−3.61 (m, 4H), 3.0 (t, J = 8.5 Hz, 2H), 2.65 (s, 3H), 2.2−2.3 (m, 2H). ^{31}P NMR (D_2O): δ 17.75.

1-Hydroxy-3-(3-phenyltetrahydrothiophenium-1-yl)propylidene-1,1-bisphosphonic Acid (28). Compound **28** was prepared from 3-phenyltetrahydrothiophene (0.75, 4.57 mmol) following General Methods B and C (205 mg, 4.6 mmol, 10%). Anal. ($C_{13}H_{19}O_6NaP_2S\cdot2.5H_2O$). ^{1}H NMR (400 MHz, D_2O): δ 7.12−7.3 (m, 5H), 3.45 (t, J = 7.8 Hz, 2H), 2.7 (s, 6H), 3.00−3.10 (m, 2H), 2.0−2.2 (m, 4H), 1.75−1.98 (m, 4H). ^{31}P NMR (D_2O): δ 18.05.

2-[Methyl 4-(3-carboxypropyl)phenybutylsulfonium-1-yl]ethylidene-1,1-bisphosphonic Acid (29). Compound **29** was prepared from methyl 4-(3-carboxypropyl)phenybutyl sulfide (0.75 g, 2.8 mmol) and vinylidene-1,1-diphosphonic acid (0.44 g, 2.3 mmol) following General Method D (0.75 g, 1.65 mmol, 72%). Anal. ($C_{17}H_{28}O_8P_2S\cdot0.5H_2O$) C, H. ^{1}H NMR (400 MHz, D_2O): δ 77.21 (s, 4H), 3.20−3.40 (m, 2H), 3.10−3.20 (m, 1H), 2.95−3.00 (m, 1H), 2.63 (s, 3H), 2.45−2.60 (m, 4H), 2.06 (t, J = 6.9 Hz), 1.95−2.0 (m, 1H), 1.55−1.75 (m, 6H). ^{31}P NMR (D_2O): δ 15.01 (d, J = 17.4 Hz).

2-(Methyl, dodecylsulfonium-1-yl)ethylidene-1,1-bisphosphonic Acid (30). Compound **30** was prepared from methyl dodecyl sulfide (0.52 g, 2.4 mmol)and vinylidene-1,1-diphosphonic acid (380 mg, 2 mmol) following General Method D (554 mg, 1.17 mmol, 58%). Anal. ($C_{15}H_{34}O_6P_2S\cdot0.3H_2O$) C, H. ^{1}H NMR (400 MHz, D_2O): δ 3.30−3.50 (m, 2H), 3.10−3.20 (m, 1H), 2.90−3.00 (m, 1H), 2.66 (s, 3H), 1.90−2.05 (m, 1H), 1.60−1.70 (m, 2H), 1.22−1.34 (m, 2H), 1.02−1.20 (m, 16H), 0.73 (t, J = 6.5 Hz, 3H). ^{31}P NMR (D_2O): δ 15.02 (dd, J = 4.4, 19.7 Hz).

2-(Methyl, decylsulfonium-1-yl)ethylidene-1,1-bisphosphonic Acid (31). Compound **31** was prepared from methyl decyl sulfide (450 mg, 2.4 mmol) and vinylidene-1,1-diphosphonic acid (380 mg, 2 mmol) following General Method D (535 mg, 1.4 mmol, 70%). Anal. ($C_{13}H_{30}O_6P_2S\bullet0.3H_2O$) C, H. ^{1}H NMR (400 MHz, D_2O): δ 3.30−3.50 (m, 2H), 3.10−3.20 (m, 1H), 2.90−3.00 (m, 1H), 2.63 (s, 3H), 1.90−2.05 (m, 1H), 1.62−1.70 (m, 2H), 1.22−1.34 (m, 2H), 1.00−1.20 (m, 14H), 0.69 (t, J = 6.5 Hz, 3H). ^{31}P NMR (D_2O): δ 15.01 (dd, J = 4.4, 19.7 Hz).

2-(Methyl, tetradecylsulfonium-1-yl)ethylidene-1,1-bisphosphonic Acid (32). Compound **32** was prepared from methyl tetradecyl sulfide (586 mg, 2.4 mmol) and vinylidene-1,1-diphosphonic acid (380 mg, 2 mmol) following General Method D (590 mg, 1.34 mmol, 67%). Anal. ($C_{17}H_{38}O_6P_2S\cdot0.5H_2O$) C, H. ^{1}H NMR (400 MHz, D_2O): δ 3.30−3.50 (m, 2H), 3.10−3.20 (m, 1H), 2.90−3.00 (m, 1H), 2.66 (s, 3H), 1.90−2.05 (m, 1H), 1.60−1.70 (m, 2H), 1.22−1.34 (m, 2H), 1.02−1.20 (m, 20H), 0.82 (t, J = 6.5 Hz, 3H). ^{31}P NMR (D_2O): δ 15.51 (d, J 15.7 Hz).

2-(Methyl, tridecylsulfonium-1-yl)ethylidene-1,1-bisphosphonic Acid (33). Compound **33** was prepared from methyl tridecyl sulfide (550 mg, 2.4 mmol) and vinylidene-1,1-diphosphonic acid (380 mg, 2 mmol) following General Method D (517 mg, 1.18 mmol, 59%). Anal. ($C_{16}H_{36}O_6P_2S\cdot1.2H_2O$) C, H. ^{1}H NMR (400 MHz, D_2O): δ 3.30−3.51 (m, 2H), 3.10−3.20 (m, 1H), 2.91−3.00 (m, 1H), 2.75 (s, 3H), 1.91−2.00 (m, 1H), 1.60−1.70 (m, 2H), 1.25−1.35 (m, 2H), 1.02−1.20 (m, 18H), 0.84 (t, J = 6.5 Hz, 3H). ^{31}P NMR (D_2O): δ 15.41 (d, J 15.7 Hz).

2-(Methyl, undecylsulfonium-1-yl)ethylidene-1,1-bisphosphonic Acid (34). Compound **34** was prepared from methyl undecyl sulfide (485 mg, 2.4 mmol) and vinylidene-1,1-diphosphonic acid (380 mg, 2 mmol) following General Method D (579 mg, 1.43 mmol, 71%). Anal. ($C_{14}H_{32}O_6P_2S\cdot H_2O$) C, H. ^{1}H NMR (400 MHz, D_2O): δ 3.30−3.51 (m, 2H), 3.10−3.20 (m, 1H), 2.91−3.00 (m, 1H), 2.75 (s, 3H), 1.91−2.00 (m, 1H), 1.60−1.70 (m, 2H), 1.25−1.35 (m, 2H), 1.02−1.20 (m, 14H), 0.80 (t, J = 6.5 Hz, 3H). ^{31}P NMR (D_2O): δ 15.41 (d, J 15.7 Hz).

2-(Methyl, licosylsulfonium-1-yl)ethylidene-1,1-bisphosphonic Acid (35). Compound **35** was prepared from methyl icosyl sulfide (780 mg, 2.4 mmol) and vinylidene-1,1-diphosphonic acid (380 mg, 2 mmol) following General Method D (892 mg, 1.62 mmol, 81%). Anal. ($C_{23}H_{49}NaO_6P_2S\cdot0.7H_2O$) C, H. ^{1}H NMR (400 MHz, D_2O): δ 3.31−3.53 (m, 2H), 3.12−3.20 (m, 1H), 2.90−3.00 (m, 1H), 2.69 (s, 3H), 1.90−2.00 (m, 1H), 1.60−1.70 (m, 2H), 1.22−1.34 (m, 2H), 1.02−1.20 (m, 32H), 0.78 (t, J = 6.5 Hz, 3H). ^{31}P NMR (D_2O): δ 15.41 (d, J 15.7 Hz).

2-(Methyl, octadecylsulfonium-1-yl)ethylidene-1,1-bisphosphonic Acid (36). Compound **36** was prepared from methyl octadecyl sulfide (720 mg, 2.4 mmol) and vinylidene-1,1-diphosphonic acid (380 mg, 2 mmol) following General Method D (645 mg, 1.18 mmol, 59%). Anal. ($C_{21}H_{44}Na_2O_6P_2S\cdot H_2O$) C, H. ^{1}H NMR (400 MHz, D_2O): δ 3.31−3.53 (m, 2H), 3.12−3.20 (m, 1H), 2.90−3.00 (m, 1H), 2.69 (s, 3H), 1.90−2.00 (m, 1H), 1.60−1.70 (m, 2H), 1.22−1.34 (m, 2H), 1.02−1.20 (m, 28H), 0.82 (t, J = 6.5 Hz, 3H). ^{31}P NMR (D_2O): δ 15.41 (d, J 15.7 Hz).

2-(Methyl, hexadecylsulfonium-1-yl)ethylidene-1,1-bisphosphonic Acid (37). Compound **37** was prepared from methyl hexadecyl sulfide (650 mg, 2.4 mmol) and vinylidene-1,1-diphosphonic acid (380 mg, 2 mmol) following General Method D (630 mg, 1.31 mmol, 65%). Anal. ($C_{19}H_{42}O_6P_2S\cdot1.2H_2O$) C, H. ^{1}H NMR (400 MHz, D_2O): δ 3.31−3.53 (m, 2H), 3.12−3.20 (m, 1H), 2.90−3.00 (m, 1H), 2.69 (s, 3H), 1.90−2.00 (m, 1H), 1.60−1.70 (m, 2H), 1.22−1.34 (m, 2H), 1.02−1.20 (m, 24H), 0.82 (t, J = 6.5 Hz, 3H). ^{31}P NMR (D_2O): δ 15.41 (d, J 15.7 Hz).

2-(Methyl, octylsulfonium-1-yl)ethylidene-1,1-bisphosphonic Acid (38). Compound **38** was prepared from methyl octyl sulfide (384 mg, 2.4 mmol) and vinylidene-1,1-diphosphonic acid (380 mg, 2 mmol) following General Method D (480 mg, 1.38 mmol, 69%). Anal. ($C_{11}H_{26}O_6P_2S$) C, H. ^{1}H NMR (400 MHz, D_2O): δ 3.3−3.47 (m, 2H), 3.13−3.21(m, 1H), 2.9−3.0 (m, 1H), 2.66 (s, 3H), 1.90−2.00 (m, 1H), 1.52−1.57 (m, 2H), 1.27−1.37 (m, 2H), 1.02−1.25 (m, 8H), 0.72 (t, J = 6.5 Hz, 3H). ^{31}P NMR (D_2O): δ 15.23.

1-Hydroxy-3-(methyl, octylsulfonium-1-yl)propylidene-1,1-bisphosphonic Acid (39). Compound **39** was prepared from methyl octyl sulfide (480 mg, 3 mmol) following General Methods B and C (152 mg, 0.36 mmol, 12%). ^{1}H NMR (400 MHz, D_2O): ^{1}H NMR

(400 MHz, D_2O): δ 3.00−3.41 (m, 4H), 2.69 (s, 3H), 2.2−2.3 (m, 2H), 1.60−1.75 (m, 2H), 1.15−1.37 (m, 10H), 0.77 (t, $J = 7.5$ Hz, 3H). ^{31}P NMR (D_2O): δ 17.57.

1-Hydroxy-2-(methyl, propylsulfonium-1-yl)ethylidene-1,1-bisphosphonic Acid (40). Compound **40** was prepared from methyl propyl sulfide (220 mg, 2.4 mmol) following General Methods A and C (82 mg, 0.21 mmol, 9%). Anal. ($C_6H_{16}O_7P_2S\cdot1.3H_2O$) C, H. ^{1}H NMR (400 MHz, D_2O): δ 3.30−3.50 (m, 2H), 2.90−3.20 (m, 2H), 2.71 (s, 3H), 1.62−1.73 (m, 2H), 0.93 (t, $J = 6.5$ Hz, 3H). ^{31}P NMR (D_2O): δ 15.24.

2-(Methyl, propylsulfonium-1-yl)ethylidene-1,1-bisphosphonic Acid (41) Compound **41** was prepared from methyl propyl sulfide (360 mg, 4 mmol) and vinylidene-1,1-diphosphonic acid (380 mg, 2 mmol) following General Method D (272 mg, 0.95 mmol, 49%). Anal. ($C_6H_{16}O_6P_2S$) C, H. ^{1}H NMR (400 MHz, D_2O): δ 3.25−3.50 (m, 2H), 3.15−3.20 (m, 1H), 2.90−3.03 (m, 1H), 2.67 (s, 3H), 1.92−2.05 (m, 1H), 1.62−1.71 (m, 2H), 0.91 (t, $J = 6.5$ Hz, 3H). ^{31}P NMR (D_2O): δ 15.01.

1-Hydroxy-3-(dimethylsulfonium-1-yl)propylidene-1,1-bisphosphonic Acid (42). Compound **42** was prepared from dimethyl sulfide (0.4 g, 6.4 mmol) following General Methods B and C (172 mg, 0.58 mmol, 9%). Anal. ($C_5H_4O_7P_2S\cdot0.5CH_3OH$). ^{1}H NMR (400 MHz, D_2O): δ 3.45 (t, $J = 7.8$ Hz, 2H), 2.7 (s, 6H), 3.00−3.10 (m, 2H), 2.0−2.2 (m, 4H), 1.75−1.98 (m, 4H). ^{31}P NMR (D_2O): δ 19.88.

1-Hydroxy-2-(dimethylsulfonium-1-yl)ethylidene-1,1-bisphosphonic Acid (43). Compound **43** was prepared from dimethyl sulfide (1.5 g, 2.4 mmol) following General Methods A and C (447 mg, 1.7 mmol, 7%). Anal. ($C_4H_{12}O_7P_2S$) C, H. ^{1}H NMR (400 MHz, D_2O): δ 3.50−3.61 (m, 4H), 2.7 (s, 6H). ^{31}P NMR (D_2O): δ 15.6.

2-(Methyl, pentylsulfonium-1-yl)ethylidene-1,1-bisphosphonic Acid (44). Compound **44** was prepared from methyl pentyl sulfide (283 mg, 2.4 mmmol) and vinylidene-1,1-diphosphonic acid (380 mg, 2 mmol) following General Method D (427 mg, 1.34 mmol, 67%). Anal. ($C_8H_{20}O_6P_2S\cdot0.7H_2O$) C, H. ^{1}H NMR (400 MHz, D_2O): δ 3.23−3.43 (m, 2H), 3.15−3.21(m, 1H), 2.90−3.03 (m, 1H), 2.77 (s, 3H), 1.90−2.00 (m, 1H), 1.62−1.77 (m, 2H), 1.27−1.37 (m, 2H), 1.12−1.25 (m, 2H), 0.74 (t, $J = 6.5$ Hz, 3H). ^{31}P NMR (D_2O): δ 14.93.

1-Hydroxy-3-(methyl, pentenylsulfonium-1-yl)propylidene-1,1-bisphosphonic Acid (45). Compound **45** was prepared from methyl pentyl sulfide (0.7 g, 5.9 mmol) following General Methods B and C (158 mg, 0.41 mmol, 7%). Anal. ($C_{13}H_{13}NaO_7P_2S$) C, H, N. ^{1}H NMR (400 MHz, D_2O): δ 3.06−3.49 (m, 4H), 2.72 (s, 3H), 2.2−2.3 (m, 2H), 1.60−1.75 (m, 2H), 1.15−1.25 (m, 2H), 1.30−1.37 (m, 2H), 0.72 (t, $J = 7.5$ Hz, 3H). ^{31}P NMR (D_2O): δ 17.57.

1-Hydroxy-3-(methyl, propylsulfonium-1-yl)propylidene-1,1-bisphosphonic Acid (46). Compound **46** was prepared from methyl propyl sulfide (0.5 g, 5.6 mmol) following General Methods B and C (148 mg, 0.42 mmol, 8%). Anal. ($C_7H_{17}NaO_7P_2S$) C, H. ^{1}H NMR (400 MHz, D_2O): δ 3.00−3.52 (m, 4H), 2.75 (s, 3H), 2.1−2.3 (m, 2H), 1.53−1.70 (m, 2H), 1.23−1.35 (m, 2H), 0.78 (t, $J = 7.5$ Hz, 3H). ^{31}P NMR (D_2O): δ 17.79.

Cell Growth Inhibition Assays. Human tumor cell lines MCF-7 (breast adenocarcinoma), NCI-H460 (lung large cell), and SF-268 (central nervous system glioblastoma) were obtained from the National Cancer Institute and maintained at 100% humidity and 5% CO_2 at 37 °C. Cell lines were cultured in RPMI-1640 medium supplemented with 2 mM L-glutamine and 10% fetal bovine serum (Gibco, Grand Island, NY) at 37 °C in a 5% CO_2 atmosphere with 100% humidity. Compound stock solutions were typically prepared in water at a concentration of 0.01 M. A broth microdilution method was used to determine the bisphosphonate growth inhibition IC_{50} values. Compounds were half log serial diluted using cell culture media into 96-well TC-treated flat bottom plates (Corning Inc., Corning, NY) typically from 316 μM to 10nM, but in some cases compounds were run over a larger concentration range to enable accurate IC_{50} determinations. Cells were plated at a density of 5000 cells/well. Cells were then incubated under the same culture conditions for 4 days at which time an MTT ((3-(4,5-dimethylthiazole-2-yl)-2,5-diphenyltetrazolium bromide) cell proliferation assay (ATCC, Manassas, VA) was performed to obtain dose response curves. Briefly, cells were incubated for 2 h under culture conditions with the tetrazolium salt, lysed with detergent, incubated overnight, protected from light at room temperature. The absorbance at 600 nm was read the following day using a SpectraMax Plus 384 spectrophotometer (Molecular Devices, Sunnyvale, CA). The compound concentration for 50% growth inhibition values (IC_{50}) were obtained by fitting absorbance data to a rectangular hyperbolic function: $I = (I_{max})(C)/IC_{50} + C$ where I is the percent inhibition, $I_{max} = 100\%$ inhibition and C is the concentration of the inhibitor, using GraphPad PRISM 3.0 software for windows (Graphpad Software Inc., San Diego, CA).

Computational Methods. To relate the activity of the sulfonium bisphosphonates to their chemical structure, we used four computational methods: 2D-QSAR, hologram QSAR (HQSAR),[40] comparative molecular similarity indices analysis (CoMSIA),[46] and pharmacophore modeling. For molecular descriptor QSAR, chemical structures were imported into the Molecular Operating Environment (MOE)[37] program, 3D structures were generated, and >200 2D and 3D molecular descriptors were computed. Alignment of molecules is not required for this method. The AutoQuaSAR[38] module was then used to systematically evaluate molecular descriptor space in a stepwise fashion, building a series of cross-validated partial least-squares (PLS) models using combinations of the descriptors while monitoring the r^2 and cross-validated r^2 (q^2) trajectory. Models with the fewest number of components (descriptors) and maximum predictive ability (r^2, q^2) where then evaluated manually, for chemical significance. The final model selected included terms accounting for the number of contiguous rotatable bonds, molar refractivity (SMR VSA7),[39,47] partial positive charge (PEOE VSA+2),[39,48] and molecular compactness (Weiner Path).[49]

Hologram QSAR (HQSAR).[40] Chemical structures were imported into Sybyl 7.11 (Tripos Inc., St. Louis, MO) along with activity data. Molecular holograms were computed using hologram lengths of 97, 151, 199, 257, 307, and 353 and fragments of four to seven atoms, with atom, bond, and connection information. The best models were chosen based on the highest cross-validated r^2.

CoMSIA[46] analysis was performed in the Sybyl 7.3[50] program using default settings. All alignments for the compounds were prepared in the program MOE.[37] Three-dimensional energy minimized structures were generated and two alignments constructed, one using the maximum common substructure (MCS) approach, the second utilizing the flexible alignment module within MOE. The MCS approach was carried out manually on the energy-minimized structures, with the energy-minimized structure of the most active molecule serving as the template. For the flexible alignment method, molecules were added sequentially to the alignment, performing up to 1000 flexible refinement iterations using a gradient test of 0.01 to 1.0 with hydrophobe, logP, and partial charge similarity features used in addition to the default options (H-bond donor, acceptor, aromaticity, polar hydrogens, and volume). The alignments were then exported into the Sybyl 7.3[50] program, where atomic charges were determined by using the Gasteiger−Marsili method.[48] CoMSIA indices were calculated on a rectangular grid containing each of the sets of aligned molecules using steric, electrostatic, hydrophobic, donor, and acceptor fields. Default grid spacing and probe atoms were used. To relate the structural features to activity, a partial least-squares analysis was applied. The optimal number of components for each model was determined by using SAMPLS[51] cross-validation. Test-set validations and scrambling stability analyses were then performed using Sybyl 7.3.

A common feature pharmacophore model was constructed in MOE[37] using the consensus pharmacophore module and the polarity-charge-hydrophobicity (PCH) scheme. The final pharmacophore was generated from energy-minimized structures of the top most active compounds using consensus features suggested by the algorithm: hydrophobic, aromatic, cationic, and a combination of features representing the phosphonate groups (acceptor, anion, and metal ligator). These features representing the phosphonate

groups were combined using logical expressions within MOE to produce two master features, each mapping to a phosphonate group. Tolerances (sizes) of the spheres encompassing the features were uniformly enlarged slightly to relax the model.

Molecular docking was performed using the Glide 4.5[45] program within the Maestro 8.0[52] interface. The target proteins were prepared using the protein preparation wizard. Hydrogens were added, Mg ions present in the active site were assigned a +2 charge, and waters beyond 5 Å of the heterogroups were deleted. Hydrogen bonds were optimized and the hydrogen positions minimized to the default value. The receptor grid was generated from the prepared target structures using the default parameters, with additional constraints added for each Mg^{2+}, and two hydrophobic constraints at the end of the hydrophobic tunnel present in FPPS. Any, all, or none of these constraints can be activated during the docking calculation. Ligands were imported as SD files, with atom types and bond orders verified. Ligands were then minimized using the MacroModel multiple minimization module in Maestro 8.0.[52] Docking calculations were performed specifying standard precision, together with constraints enabled requiring interactions with at least two Mg^{2+} ions. The final results were visualized using the Glide pose viewer.

Conclusions

The results we have described above are of interest for a number of reasons. First, we have synthesized a broad range of novel sulfonium bisphosphonates. Second, we have tested these bisphosphonates as growth inhibitors of three human tumor cell lines (MCF-7, NCI-H460, and SF-268). The most active species were found to have IC_{50} values in the 200 nM range and are considerably more active than any other bisphosphonates, such as minodronate, zoledronate, risedronate, ibandronate, alendronate, and pamidronate. Third, we carried out a series of QSAR investigations of these compounds and showed that their activities can be predicted within a factor of ~2, using CoMSIA methods, obtaining similar results from both maximum common substructure and feature-based alignments. Fourth, we report the first X-ray crystallographic structures of sulfonium bisphophonate−FPPS complexes, together with additional (docking) results, which indicate how other bisphosphonates bind to FPPS. Overall, the observation that these novel cationic bisphosphonates have high activity against three tumor cell lines is of general interest, and suggests that these and other, related species, may be of interest in the context of new anticancer therapies and potentially as antiinfectives.

Acknowledgment. This work was supported by the United States Public Health Service (NIH grant GM-073216). YZ was supported by a Postdoctoral Fellowship from the American Heart Association, Midwest Affiliate. A.L. was supported by an NIH Institutional NRSA in Molecular Biophysics (NIH Training Grant GM-08276). We thank Howard Robinson of Brookhaven National Laboratories for obtaining the X-ray diffraction data. We also thank Schrödinger, LLC for providing evaluation licenses of Glide.

Supporting Information Available: Supporting methods, figures, and tables, including microanalysis data, human FPPS and molecular diameter, 2D-QSAR output, hologram QSAR results, and CoMSIA results. This material is available free of charge via the Internet at http://pubs.acs.org.

References

(1) Shipman, C. M.; Croucher, P. I.; Russell, R. G.; Helfrich, M. H.; Rogers, M. J. The bisphosphonate incadronate (YM175) causes apoptosis of human myeloma cells in vitro by inhibiting the mevalonate pathway. *Cancer Res.* **1998**, *58* (23), 5294−7.

(2) Shipman, C. M.; Rogers, M. J.; Apperley, J. F.; Russell, R. G.; Croucher, P. I. Bisphosphonates induce apoptosis in human myeloma cell lines: a novel anti-tumour activity. *Br. J. Haematol.* **1997**, *98* (3), 665−72.

(3) Morgan, C.; Lewis, P. D.; Jones, R. M.; Bertelli, G.; Thomas, G. A.; Leonard, R. C. The in vitro anti-tumour activity of zoledronic acid and docetaxel at clinically achievable concentrations in prostate cancer. *Acta Oncol.* **2007**, *46* (5), 669−77.

(4) Issat, T.; Nowis, D.; Legat, M.; Makowski, M.; Klejman, M. P.; Urbanski, J.; Skierski, J.; Koronkiewicz, M.; Stoklosa, T.; Brzezinska, A.; Bil, J.; Gietka, J.; Jakobisiak, M.; Golab, J. Potentiated antitumor effects of the combination treatment with statins and pamidronate in vitro and in vivo. *Int. J. Oncol.* **2007**, *30* (6), 1413−25.

(5) Koshimune, R.; Aoe, M.; Toyooka, S.; Hara, F.; Ouchida, M.; Tokumo, M.; Sano, Y.; Date, H.; Shimizu, N., Anti-tumor effect of bisphosphonate (YM529) on non-small cell lung cancer cell lines. *BMC Cancer* **2007**, *7*, 8.

(6) Kubo, T.; Shimose, S.; Matsuo, T.; Tanaka, K.; Yasunaga, Y.; Sakai, A.; Ochi, M. Inhibitory effects of a new bisphosphonate, minodronate, on proliferation and invasion of a variety of malignant bone tumor cells. *J. Orthop. Res.* **2006**, *24* (6), 1138−44.

(7) Dieli, F.; Vermijlen, D.; Fulfaro, F.; Caccamo, N.; Meraviglia, S.; Cicero, G.; Roberts, A.; Buccheri, S.; D'Asaro, M.; Gebbia, N.; Salerno, A.; Eberl, M.; Hayday, A. C. Targeting human gd T cells with zoledronate and interleukin-2 for immunotherapy of hormone-refractory prostate cancer. *Cancer Res.* **2007**, *67* (15), 7450−7.

(8) Sato, K.; Yuasa, T.; Nogawa, M.; Kimura, S.; Segawa, H.; Yokota, A.; Maekawa, T., A third-generation bisphosphonate, minodronic acid (YM529), successfully prevented the growth of bladder cancer in vitro and in vivo. *Br. J. Cancer* **2006**, *95* (10), 1354−61.

(9) Rodriguez, N.; Bailey, B. N.; Martin, M. B.; Oldfield, E.; Urbina, J. A.; Docampo, R. Radical Cure of Experimental Cutaneous Leishmaniasis by the Bisphosphonate Pamidronate. *J. Infect. Dis.* **2002**, *186* (1), 138−140.

(10) Leon, A.; Liu, L.; Yang, Y.; Hudock, M. P.; Hall, P.; Yin, F.; Studer, D.; Puan, K. J.; Morita, C. T.; Oldfield, E. Isoprenoid biosynthesis as a drug target: bisphosphonate inhibition of Escherichia coli K12 growth and synergistic effects of fosmidomycin. *J. Med. Chem.* **2006**, *49* (25), 7331−41.

(11) Wilhelm, M.; Kunzmann, V.; Eckstein, S.; Reimer, P.; Weissinger, F.; Ruediger, T.; Tony, H. P., $\gamma\delta$ T Cells for Immune Therapy of Patients with Lymphoid Malignancies. *Blood* **2003**, *102* (1), 200−6.

(12) Sato, K.; Kimura, S.; Segawa, H.; Yokota, A.; Matsumoto, S.; Kuroda, J.; Nogawa, M.; Yuasa, T.; Kiyono, Y.; Wada, H.; Maekawa, T. Cytotoxic effects of gammadelta T cells expanded ex vivo by a third generation bisphosphonate for cancer immunotherapy. *Int. J. Cancer* **2005**, *116* (1), 94−9.

(13) Das, H.; Wang, L.; Kamath, A.; Bukowski, J. F., Vgamma2Vdelta2 T-cell receptor-mediated recognition of aminobisphosphonates. *Blood* **2001**, *98* (5), 1616−8.

(14) Wang, L.; Kamath, A.; Das, H.; Li, L.; Bukowski, J. F., Antibacterial Effect of Human Vγ2Vδ2 T Cells *In vivo*. *J. Clin. Invest.* **2001**, *108* (9), 1349−57.

(15) Reszka, A. A.; Rodan, G. A., Nitrogen-containing bisphosphonate mechanism of action. *Mini Rev. Med. Chem.* **2004**, *4* (7), 711−9.

(16) Fleisch, H.; Russell, R. G.; Francis, M. D. Diphosphonates Inhibit Hydroxyapatite Dissolution in vitro and Bone Resorption in Tissue Culture and in vivo. *Science* **1969**, *165*, 1262−1264.

(17) Lehenkari, P. P.; Kellinsalmi, M.; Napankangas, J. P.; Ylitalo, K. V.; Monkkonen, J.; Rogers, M. J.; Azhayev, A.; Vaananen, H. K.; Hassinen, I. E. Further Insight Into Mechanism of Action of Clodronate: Inhibition of Mitochondrial ADP/ATP Translocase by a Nonhydrolyzable, Adenine-Containing Metabolite. *Mol. Pharmacol.* **2002**, *61* (5), 1255−62.

(18) Monkkonen, H.; Auriola, S.; Lehenkari, P.; Kellinsalmi, M.; Hassinen, I. E.; Vepsalainen, J.; Monkkonen, J. A new endogenous ATP analog (ApppI) inhibits the mitochondrial adenine nucleotide translocase (ANT) and is responsible for the apoptosis induced by nitrogen-containing bisphosphonates. *Br. J. Pharmacol.* **2006**, *147* (4), 437−45.

(19) Cromartie, T. H.; Fisher, K. J.; Grossman, J. N. The discovery of a novel site of action for herbicidal bisphosphonates. *Pestic. Biochem. Physiol.* **1999**, *63* (2), 114−126.

(20) Martin, M. B.; Arnold, W.; Heath, H. T., 3rd; Urbina, J. A.; Oldfield, E., Nitrogen-Containing Bisphosphonates as Carbocation Transition State Analogs for Isoprenoid Biosynthesis. *Biochem. Biophys. Res. Commun.* **1999**, *263* (3), 754−8.

(21) Bergstrom, J. D.; Bostedor, R. G.; Masarachia, P. J.; Reszka, A. A.; Rodan, G. Alendronate is a specific, nanomolar inhibitor of farnesyl diphosphate synthase. *Arch. Biochem. Biophys.* **2000**, *373* (1), 231−41.

(22) Grove, J. E.; Brown, R. J.; Watts, D. J. The intracellular target for the antiresorptive aminobisphosphonate drugs in Dictyostelium discoideum is the enzyme farnesyl diphosphate synthase. *J. Bone Miner. Res.* **2000**, *15* (5), 971−81.

(23) Luckman, S. P.; Hughes, D. E.; Coxon, F. P.; Graham, R.; Russell, G.; Rogers, M. J., Nitrogen-containing bisphosphonates inhibit the mevalonate pathway and prevent post-translational prenylation of GTP-binding proteins, including Ras. *J. Bone Miner. Res.* **1998**, *13* (4), 581−9.
(24) Dunford, J. E.; Rogers, M. J.; Ebetino, F. H.; Phipps, R. J.; Coxon, F. P. Inhibition of protein prenylation by bisphosphonates causes sustained activation of Rac, Cdc42, and Rho GTPases. *J. Bone Miner. Res.* **2006**, *21* (5), 684−94.
(25) Kavanagh, K. L.; Guo, K.; Dunford, J. E.; Wu, X.; Knapp, S.; Ebetino, F. H.; Rogers, M. J.; Russell, R. G.; Oppermann, U. The molecular mechanism of nitrogen-containing bisphosphonates as antiosteoporosis drugs. *Proc. Natl. Acad. Sci. U.S.A.* **2006**, *103* (20), 7829−34.
(26) Rondeau, J. M.; Bitsch, F.; Bourgier, E.; Geiser, M.; Hemmig, R.; Kroemer, M.; Lehmann, S.; Ramage, P.; Rieffel, S.; Strauss, A.; Green, J. R.; Jahnke, W. Structural basis for the exceptional in vivo efficacy of bisphosphonate drugs. *ChemMedChem* **2006**, *1* (2), 267−73.
(27) Hosfield, D. J.; Zhang, Y.; Dougan, D. R.; Broun, A.; Tari, L. W.; Swanson, R. V.; Finn, J. Structural Basis for Bisphosphonate-Mediated Inhibition of Isoprenoid Biosynthesis. *J. Biol. Chem.* **2004**, *279* (10), 8526−9.
(28) Mao, J.; Mukherjee, S.; Zhang, Y.; Cao, R.; Sanders, J. M.; Song, Y.; Zhang, Y.; Meints, G. A.; Gao, Y. G.; Mukkamala, D.; Hudock, M. P.; Oldfield, E., Solid-state NMR, crystallographic, and computational investigation of bisphosphonates and farnesyl diphosphate synthase-bisphosphonate complexes. *J. Am. Chem. Soc.* **2006**, *128* (45), 14485−97.
(29) Sheng, L. S.; Horning, E. C.; Horning, M. G. Synthesis and Elimination-Reactions of Methylsulfonium Ions Formed from Styrene Oxide and Methylthio Compounds Related to Methionine and Cysteine. *Drug Metab. Dispos.* **1984**, *12* (3), 297−303.
(30) Sano, Y.; Yamada, H. Progress in suplatast tosilate research. *Clin. Exp. Allergy* **2007**, *37* (7), 970−2.
(31) Yanagihara, Y.; Kiniwa, M.; Ikizawa, K.; Yamaya, H.; Shida, T.; Matsuura, N.; Koda, A.; Suppression, of Ige, Production, by Ipd-1151t (Suplatast, Tosilate), a New, Dimethylsulfonium, Agent, .1. Regulation of Murine Ige Response. *Jpn. J. Pharmacol.* **1993**, *61* (1), 23−30.
(32) Zhang, Y.; Leon, A.; Song, Y.; Studer, D.; Haase, C.; Koscielski, L. A.; Oldfield, E. Activity of nitrogen-containing and non-nitrogen-containing bisphosphonates on tumor cell lines. *J. Med. Chem.* **2006**, *49* (19), 5804−14.
(33) Sanders, J. M.; Song, Y.; Chan, J. M.; Zhang, Y.; Jennings, S.; Kosztowski, T.; Odeh, S.; Flessner, R.; Schwerdtfeger, C.; Kotsikorou, E.; Meints, G. A.; Gomez, A. O.; Gonzalez-Pacanowska, D.; Raker, A. M.; Wang, H.; van Beek, E. R.; Papapoulos, S. E.; Morita, C. T.; Oldfield, E., Pyridinium-1-yl Bisphosphonates are Potent Inhibitors of Farnesyl Diphosphate Synthase and Bone Resorption. *J. Med. Chem.* **2005**, *48* (8), 2957−63.
(34) Sanders, J. M.; Ghosh, S.; Chan, J. M.; Meints, G.; Wang, H.; Raker, A. M.; Song, Y.; Colantino, A.; Burzynska, A.; Kafarski, P.; Morita, C. T.; Oldfield, E., Quantitative Structure-Activity Relationships for ©TM T Cell Activation by Bisphosphonates. *J. Med. Chem.* **2004**, *47* (2), 375−84.
(35) Widler, L.; Jaeggi, K. A.; Glatt, M.; Muller, K.; Bachmann, R.; Bisping, M.; Born, A. R.; Cortesi, R.; Guiglia, G.; Jeker, H.; Klein, R.; Ramseier, U.; Schmid, J.; Schreiber, G.; Seltenmeyer, Y.; Green, J. R. Highly Potent Feminal Bisphosphonates. From *Pamidronate disodium* (Aredia) to Zoledronic Acid (Zometa). *J. Med. Chem.* **2002**, *45* (17), 3721−38.
(36) Petitjean, M. Applications of the Radius Diameter Diagram to the Classification of Topological and Geometrical Shapes of Chemical-Compounds. *J. Chem. Inf. Comput. Sci.* **1992**, *32* (4), 331−337.
(37) *MOE*, 2006.08; Chemical Computing Group, Inc.: Montreal, Quebec, 2006.
(38) Goto, J. *AutoQuaSAR 2006.08*, Ryoka Systems, Inc.: Tokyo, Japan, 2006.
(39) Labute, P. A widely applicable set of descriptors. *J. Mol. Graph. Modelling* **2000**, *18* (4−5), 464−477.
(40) *Hologram QSAR (HQSAR) module part of Sybyl 7.11*, Tripos Inc.: St. Louis, MO.
(41) Labute, P.; Williams, C.; Feher, M.; Sourial, E.; Schmidt, J. M. Flexible alignment of small molecules. *J. Med. Chem.* **2001**, *44* (10), 1483−1490.
(42) Clark, R. D.; Sprous, D. G., Validating models based on large datasets. In *Rational Approaches to Drug Design*; Holtje, H.-D.; Sippl, W., Eds.; Prous Science SA: Barcelona, 2001; pp 475−485.
(43) *Tripos Bookshelf 7.3*, Tripos, Inc.: St. Louis, MO.
(44) Mao, J.; Gao, Y. G.; Odeh, S.; Robinson, H.; Montalvetti, A.; Docampo, R.; Oldfield, E., Crystallization and Preliminary X-ray Diffraction Study of the Farnesyl Diphosphate Synthase from *Trypanosoma brucei*. *Acta Crystallogr. Ser. D: Biol. Crystallogr.* **2004**, *60* (Pt 10), 1863−6.
(45) *Glide 4.5*, Schrodinger, Inc.: Portland, OR.
(46) Klebe, G.; Abraham, U.; Mietzner, T. Molecular Similarity Indices in a Comparative Analysis (CoMSIA) of Drug Molecules to Correlate and Predict their Biological Activity. *J. Med. Chem.* **1994**, *37* (24), 4130−46.
(47) Wildman, S. A.; Crippen, G. M. Prediction of physicochemical parameters by atomic contributions. *J. Chem. Inf. Comput. Sci.* **1999**, *39* (5), 868−873.
(48) Gasteiger, J.; Marsili, M. Iterative Partial Equalization of Orbital Electronegativity-a Rapid Access to Atomic Charges. *Tetrahedron* **1980**, *36* (22), 3219−3228.
(49) Balaban, A. T.; Chemical, Graphs, .34. 5 New Topological Indexes for the Branching of Tree-Like Graphs. *Theor. Chim. Acta* **1979**, *53* (4), 355−375.
(50) *Sybyl 7.3*, Tripos, Inc.: St. Louis, MO.
(51) Bush, B. L.; Nachbar, R. B., Sample-Distance Partial Least-Squares-Pls Optimized for Many Variables, with Application to Comfa. *J. Comput.-Aided Mol. Des.* **1993**, *7* (5), 587−619.
(52) *Maestro 8.0*, Schrodinger Inc.: Portland, OR.

JM700991K